JAERI-Tech
99-018

FLOW STUDY ON THE ESS TARGET WATER MODEL USING THE UVP METHOD

March 1999

Katsuhiro HAGA, Yasushi TAKEDA*
Gunter BAUER* and Bernd GUTTEK*

日本原子力研究所
Japan Atomic Energy Research Institute

本レポートは，日本原子力研究所が不定期に公刊している研究報告書です。
入手の問合わせは，日本原子力研究所研究情報部研究情報課（〒319－1195 茨城県那珂郡東海村）あて，お申し越しください。なお，このほかに財団法人原子力弘済会資料センター（〒319－1195 茨城県那珂郡東海村日本原子力研究所内）で複写による実費頒布をおこなっております。

This report is issued irregularly.
Inquiries about availability of the reports should be addressed to Research Information Division, Department of Intellectual Resources, Japan Atomic Energy Research Institute, Tokai-mura, Naka-gun, Ibaraki-ken 〒319－1195, Japan.

編集兼発行　日本原子力研究所

JAERI-Tech 99-018

Flow Study on the ESS Target Water Model Using the UVP Method

Katsuhiro HAGA, Yasushi TAKEDA *, Gunter BAUER * and Bernd GUTTEK **

Center for Neutron Science
Tokai Research Establishment
Japan Atomic Energy Research Institute
Tokai-mura, Naka-gun, Ibaraki-ken

(Received February 1, 1999)

The European Spallation Source (ESS) is a next generation neutron source using a proton accelerator which generates a high power proton beam of 5MW. In the conceptual design of the ESS target, the heavy liquid metal, mercury, is used as the target material to endure the high heat load caused by the spallation reaction. The mercury target container is partitioned into three inlet and one outlet channels. One of the key issues to keep its structural integrity is to suppress recirculation flows in the outlet channel so as not to lead excessive temperature rises of the mercury which will cause boiling. To investigate flow behaviors in the ESS target container, a mock-up model was fabricated with plexiglass at the Forschungszntrum Julich (KFA) in Germany. The experiments were carried out under water flow conditions. Flow velocity fields were measured with the Ultrasound Doppler Velocity Profile Method developed at the Paul Scherrer Institute (PSI) in Switzerland. In the experiments, flow rate ratios of the inlet channels (A, B, C) were changed under a constant total flow rate of 0.88L/s as 1:0:1, 2:1:2, 1:1:1, 1:2:1 and 0:1:0. The recirculation flow was observed from the velocity patterns measured under each flow rate ratio. Flow patterns in the cross section of the recirculation flow showed large vortex structures, and the length of the recirculation flow region increased with the flow rate of the bottom inlet channel. On the bases of these experimental results, it can be said that the creation of the recirculaion flow might be inevitable in this target structure of the return-flow type.

Keywords : Flow Study, ESS Target, Spallation reaction, Water Experiment,
Recirculation Flow, UVP Method, Vector Mapping

---

* Paul Scherrer Institute

* * Forschungzentrum Jülich

ＵＶＰ法を用いた水流動実験によるＥＳＳターゲットモデルの流れ場に関する研究

日本原子力研究所東海研究所中性子科学研究センター
羽賀　勝洋・武田　　靖*・Gunter BAUER*・Bernd GUTTEK**

（1999年2月1日受理）

ＥＳＳは高出力陽子加速器を用いた５MWの出力を持つ次世代の中性子源である。ＥＳＳターゲットの概念設計では、ターゲット物質の核破砕反応によって生じる大きな熱負荷に耐えるため、液体重金属である水銀をターゲット物質として使用している。水銀ターゲット容器内は３つの入口流路と１つの出口流路に分割されており、ターゲット容器の健全性を確保する上で、水銀の局部的な温度上昇による沸騰を避けるために、出口流路内で水銀の再循環領域が生じないようにすることが重要である。そこでターゲット容器内の流れ場を測定するために、ドイツのユーリッヒ研究所でアクリル製のターゲットモデルが製作された。試験流体は水銀の代わりに水を使用し、ターゲット容器内の流れ場をスイスのパウル・シェラー研究所で開発されたＵＶＰ（Ultrasound Doppler Velocity Profile Method）を用いて測定し流速ベクトル図を作成した。実験では、ターゲット容器への水の全流入量を0.88Ｌ／ｓに保持しながら、各入口流路（Ａ，Ｂ，Ｃ）の流量比率を１：０：１，２：１：２，１：１：１，１：２：１，０：１：０の５通りに変化させた。各条件下で流速分布を測定して流速ベクトル図を作成した結果、どの条件でも再循環領域が生じており、ターゲット容器下部の入口流路（流路Ｂ）の流量比率が増すに連れ、再循環領域が大きくなることが分った。この結果より、現在のターゲット容器の構造では再循環領域の生成は不可避であり、流路の隔壁を多孔状にするなどの改良が必要であると考えられる。

東海研究所：〒319-1195　茨城県那珂郡東海村白方白根2-4
＊　パウルシェラー研究所
＊＊ユーリッヒ研究所

Contents

目　　次

1. Introduction

The European Spallation Source(ESS) is a next generation neutron source using a proton accelerator which generates a high power proton beam of 5MW. High-intensity neutron beams are produced at a target by spallation reaction between target materials and the proton beam.

In the conceptual design of the ESS target, the heavy liquid metal, mercury, is used as the target material to endure the high heat load caused by the spallation reaction. One of the key issues in keeping the structural integrity of the target container is to suppress recirculation flows in the outlet channel so as not to permit an excessive temperature rise of the mercury which will cause it to boil. The results of the experimental and computational flow study conducted with the two dimensional model of the ESS target[1,2] showed that the recirculation flow is very likely to occur in the outlet channel. Based on these results, a mock-up model for a water experiment was fabricated with plexiglass at the Forschungszntrum Julich (KFA) in Germany. The target container is partitioned into three inlet and one outlet channel. Mercury flowing through horizontal inlet channels, placed at both sides and at the bottom of the container, turns at the front end of the container (beam window) and moves in the reverse direction to the inlet flow. It then flows in the outlet channel placed at the center where the spallation reactions occur. This geometry aims to prevent the creation of the recirculation region in the outlet channel while supplying sufficient coolant to the beam window, where spallation reactions occur in the target container wall.

The experiments were carried out at the Paul Scherrer Institute (PSI) in Switzerland, and flow velocity fields in the ESS target container were measured under various flow conditions using the Ultrasound Doppler Velocity Profile Method (UVP) developed at PSI. In this study, the general behaviour of the flow in the model is discussed to evaluate the validity of the present target geometry. This study was conducted as part of the ESS project and the results of this study was also submitted to KFA as ESS Report (ESS 98-76-T).

2. Experimental Set-up

Fig.1 shows the water loop used in this experiment. Water is supplied to the test section through three inlet channels. Flow meters are installed at each inlet pipes and the flow rates are regulated by the valves below the flow meters. The maximum achievable total flow rate is 2.5 L/s with the present system. Electrodes for electrolysis are also installed just above the flow meters to generate tiny gas bubbles that makes seeding better for UVP.

Fig.2 shows a cut-out view of ESS model showing the interior geometry. The manifold, shown with grey-scale color, is made of stainless steal to be used in mercury experiments in

future. Three lower pipes are the inlets of water and the upper one the outlet. The rectangular flange seen in the middle allows insertion of the gas injector system to simulate the gas injection into mercury for the pressure wave attenuation, which was not used in this study. Several projections fixed on the outlet pipe are reinforcements to sustain the weight of the manifold.

The model was made with plexiglass which also enables UVP measurement as well as flow visualization experiments. To minimize the reflection effect of ultrasound within the wall, the wall thickness was made thin to be 3mm. Fig.3 shows the flow direction of water and the dimensions of the model . The total length of the model is 653mm and the outer width is 306mm. The height is 156mm at the rear edge and 106mm at the front. The window has a round shape with the outer radius of 53mm at the center. The side walls are also rounded. Top and bottom walls are slightly inclined with the angle of 2.4 degrees to the horizontal plane. Water flows into three channels of the model through three inlet pipes of the manifold. The target container is separated into three inlet channels and one main channel with side and bottom separation plates. Two of the inlet channels are placed at the side of the model, and one is at the bottom. The cross section of the bottom channel is rectangular with the width of 200mm. The height of it decreases from 34mm to 10mm as the position goes toward the front edge. The cross section of the side channels has crescent-like shape with the width of 24mm at the center of the height. The front edge of each inlet channels works as a nozzle to cool the target window with jet flow. The experimental results obtained with the two dimensional model showed the tendency that the recirculation zone becomes larger and stronger as the inlet flow rate from the bottom channel is increased. The two additional side channels were installed with intention of making the recirculation zone small while keeping the enough cooling of the target window. They are also expected to shift the recirculation zone out of the spallation reaction zone. The water passing through the side channels flow into the main channel, where the spallation reaction occurs, at the front edge. Three water flows collide each other inside the target window so that the flow structure must be very complicated there. Thereafter the water flows backward in the main channel to the outlet.

3. Flow Velocity Measurement by UVP

Flow measurement for flow mapping was carried out using Ultrasound Doppler method [3,4]. This technique has been developed at PSI for the target R & D program, and the method to obtain two-dimensional-two-components (2D2C) velocity vector filed was established [5].

3.1 Arrangement of Measuring Lines

Designing an arrangement of measuring lines is important for flow mapping. The angle of the measuring lines to the line normal to the surface of the model must be less than the critical angle of 32.9 degrees, while the distribution of the crossing points should cover whole the flow field of interest. Fig.4 and Fig.5 show the arrangement of 48 measuring lines on the horizontal measuring plane and of 36 measuring lines on the vertical measuring plane used in this experiment. True velocity vectors are obtained at 193 crossing points and at 65 points on each measuring planes respectively.

The measuring lines on the horizontal measuring plane are placed with the separation distance of 7mm and inclined 10 degrees right and left to the datum line parallel to the target model axis, which makes the crossing angle between two measuring lines as 20 degrees. Measuring lines are forced to separate widely at some places to avoid the reinforcements attached to the surface of the model. Four measuring lines parallel to the datum line, placed on both sides, cross with slanted measuring lines at the angle of 10 degrees. These angles were determined to minimise the reflection effect. The maximum depth of the vector field from the top of the target window is 270mm. The measuring lines on the vertical measuring plane are inclined 15 degrees to the normal, and the separation distance is also 7mm.

3.2 Flow Vector Mapping

The vector maps we can obtain is a time averaged flow field in the model. It takes ca. 80ms to measure one velocity profile and 1024 velocity profiles are measured for each measuring lines. An average velocity profile for one measuring line is obtained by taking the average of these 1024 velocity profiles and the flow vector components are calculated with the average velocity values at each crossing points of the measuring lines.

The flow vector maps shown in this paper were obtained by interpolating components of those velocity vectors to the 20×20 mesh points on the horizontal plane and 20×10 mesh points on the vertical plane. Together with the vector maps, figures of streamtrace lines are also shown. These lines were drawn by simply tracing the direction of velocity vectors on the flow field. Since the flow field is three dimensional, the stream function does not have the original meaning in this case and stream lines cannot be drawn by making the contour map of the stream function.

3.3 Estimation of Vz

The velocity component of vertical direction (Vz) was calculated by the equation of continuity with the measured data set of Vx and Vy using the control volume method. It

should be noted that the calculated value of Vz is the rough estimate, because the distance between the measuring plane of 10mm, which corresponds to the mesh width on the Z direction, is relatively large to estimate Vz precisely and the boundary condition was set at the bottom wall which is apart from the lower measuring plane by 20mm. It is supposed that calculated Vz differs much from true value in a region where the flow is strongly turbulent such as just inside the target window.

4. Experiment Conditions

Table 1 shows the experiment conditions. One data set corresponds to one vector map. There are 31 data sets with different combinations of flow rate and measuring plane. The flow velocity fields were measured in the horizontal plane, the inclined plane and the vertical plane. The MP height in the second column means the height of measuring plane expressed by the distance from the base level which is the center of the model as is shown in Fig.6. The MP angle in the third column is the inclination of the measuring plane from the horizon, that means, the MP angle of 0 degree corresponds to a horizontal measuring plane. The data sets from Nr.1 to Nr.6 are trial cases to decide the best measuring line arrangement. After the measuring line arrangement was decided as Nr.7, the measurement of the flow field started systematically. The items, A, B, C in the flow rate column correspond to the inlet channels as is shown in Fig.3. The ratio of flow rates of three inlet channels were changed as 1:0:1, 2:1:2, 1:1:1, 1:2:1, 0:1:0 keeping the total flow rate constant at 0.88L/s. Flow velocity at the front edge means the average water velocity at the exit of each channels. The data sets from Nr.27 to Nr.31 are cases of the measuring plane which is slightly out of the vertical with 5 degrees inclination. It is quoted as vertical measuring plane in this study. The measuring line arrangement of ML Set Nr.8 is just the same as that of ML Set Nr.7. The difference is just the distance of the base line, which defines the position of measuring lines, from the target model surface.

5. Experimental Results

It should be noted that the flow velocity vectors shown here are the projection of real vectors to the measuring plane. Since the flow structure is highly three dimensional, the water flow in the model cannot be expressed perfectly on a two dimensional plane, but the general behavior of the total flow can be understood with two dimensional vector maps. Flow patterns observed in each flow conditions will be discussed referring to vector maps and stream trace line figures in this chapter. Table 2 shows the combination of the MP height and the inlet flow rate ratio for each figures.

5.1 Comparison of vector maps of different flow rate ratios

5.1.1 MP Height : 0mm (Fig.13 Fig.14 Fig.15)

These data sets can be compared to know the change of a flow field with a relative increase of the lower channel (channel B). The recirculation region can be clearly seen on both sides of the center line in all of these cases. The flow direction at the center line is slightly shifted and inclined to the right, which makes the recirculation region on the left side larger. Symmetry of the flow field depends on the accuracy of the flow meter of inlet channels, the symmetry of the target window, or the inlet flow condition. In this case, it is considered that the reason of the flow field asymmetry is mainly due to the asymmetry of the target window of which front surface is slightly inclined. When the flow rate of channel B is small (Fig.13), the recirculation region is small and the flow velocity is also small, which means the flow in these region is almost stagnant. The left side recirculation region begins from the depth of ca. 90mm and continues to ca. 200mm. As the flow rate of channel B increases (Fig.14 and 15), the recirculation region becomes larger and stronger. The starting depth of the region is almost the same with the case of Fig.13, but the end depth extends to ca. 300mm in Fig.14 and further (undetectable) in Fig.15.

5.1.2 MP Height : +10mm (Fig.8 Fig.9 Fig10)

Flow vectors beyond the depth of 200mm, which was not measured in Fig.13, can be seen in Fig.8. Most of the vectors directs backward in this area and recirculation on the left side is not clear. The total flow pattern is just the same with the case of MP height 0mm that the recirculation region becomes larger as the flow rate of channel B increases.

5.1.3 MP Height : -10mm (Fig.18 Fig.19 Fig20)

The recirculation is generated just inside the front end of the left side wall in Fig.18, and the size of the recirculation is the smallest in this case compared with other flow rate ratio cases. It can be clearly seen that the center of the recirculation on the left side moves backward in the Y direction and the recirculation region grows larger while the flow rate of channel B increases. There is also a recirculation on the right side, but it is weak.

5.2 Comparison of vector maps of different levels

5.2.1 Flow rate ratio 1:1:1 (Fig.9 Fig.14 Fig.19 Fig.24)

This is the base case of the series of measurement. Comparing four figures, it can be seen that the flow going to the center from side channels just inside the target window become

strong as the measuring plane goes up. This shows the flow from side channels is directed upward by the flow from channel B. The flow at the center line is inclined to the right also in these cases. The recirculation region on the left side begins from the depth of ca. 50mm in Fig.19 and it shifts backward in Fig.14 and Fig.9. It can be seen that the center of the recirculation also shifts backward as the measuring plane rises, which indicates that the recirculation region has three dimensional structure with inclined axis. The center of the recirculation on the right side is generated at the depth of ca.150mm and it seems to have the same structure with the one on the left side. In addition to the large recirculation, a small vortex is generated behind the edge of the side channels.

5.2.2 Flow rate ratio 2:1:2 (Fig.8 Fig.13 Fig.18 Fig.23)

The recirculation which can be clearly seen on both sides in Fig.18 and Fig.23 becomes small and vague in Fig.8 and Fig.13. This indicates that the strong core of the vortex exists at the lower part of the main channel and the thickness of the recirculation region is thin. In Fig.18 ,the vortex center on the left side is generated at the depth of 60mm which is the closest position compared to the cases of other flow rate ratio. The shift of the vortex center position seen in these figures also indicates the inclined vortex structure same as the former case.

5.2.3 Flow rate ratio 1:2:1 (Fig.10, Fig.15, Fig.20 Fig.25)

This flow pattern is characterised by the large recirculation region ranging from just inside the target window to the depth of more than 300mm. It also can be noticed that the high velocity flow from the side channels A, C is not seen at the lower measuring plane in Fig.20, whereas it is clearly shown at the middle and upper measuring plane in Fig.15 and Fig.10. These patterns show that all of the flow from side channels are completely directed upward by the flow blowing from bottom channel and the recirculation at the lower place is not disturbed by the side channel flows. The center of the recirculaion on the left side shifts backward from the depth of 220mm to 300mm as the MP height rises also in this case, and it can be assumed that the inclined vortex region exists covering almost whole the part on the left side in the model.

5.2.4 Flow rate ratio 0:1:0 (Fig.11, Fig.16, Fig.21 Fig.26)

This is the same case with the experiment of two dimensional model, in which water was supplied to the model only through the bottom channel. The flow field from the depth of 180mm to 270mm is not shown in Fig.11, Fig16 and Fig21, because the fluctuation of the velocity data is so large in this area that the data correction has not finished. The large

vectors inside the target window in Fig.11 correspond to the direct stream from the bottom channel. The vectors near the center line of the model show there is a backward stream in the upper measuring plane. As the measuring plane goes down, the backward stream disappears in Fig.16 and 21 and only the frontward and sideward stream becomes dominant. This shows there is a large vertical recirculation ranging from the bottom to the top of the main channel. just the same with the flow observed in two dimensional model. But in this case, the side wall is rounded and it generates spanwise flow making the total flow field more complicated. Considering that the main stream is shifted to the right also in this case as well and there are no side channel flows, the asymmetry of the flow in the main channel may be caused by the asymmetry of the target window.

5.2.5 Flow rate ratio 1:0:1 (Fig.7, Fig.12, Fig.17 Fig.22)

This case is categorised as counter-flow jet stream. Contrary to expectations, the measured flow was strongly asymmetric. The flow from side channel C covers almost whole the flow field making a large recirculation region in the middle of the main channel, and the flow from side channel A is pushed back and flows along the right side wall. This flow pattern may be caused by the asymmetry of the target window. It can be assumed that the asymmetric flow fields observed in other cases were generated mainly by side channel flows and the bottom channel flow acts as a disturbance to break the asymmetric recirculation.

5.3 Spanwise motion

Fig.27 to Fig.31 shows the flow fields on the vertical measuring plane which is the vertical cross section at the depth of 100mm from the front of the target window. Two counter rotating vortices are shown on both sides of the center line ranging from the bottom to the top wall of the main channel in Fig.28, Fig.29 and Fig.30. The vortex on the left side rotating clock-wise is bigger than the one on the right side, which corresponds to the asymmetric flow observed on the horizontal measuring plane. The rotating direction is not affected by the change of the flow rate ratio. In Fig.27, the stream from channel C crosses middle of the main channel, impinges on the side wall, and generates two vortices on upper and lower side of the main channel. Since the flow from the side channel is asymmetric with respect to the horizontal center line of the main channel, the stream is shifted above the center line making the lower vortex larger. Fig.31 shows counter-rotating small vortices at the upper side of the main channel. Considering that this flow pattern was observed also in the experiment of two dimensional flow[2], in which there are no side channel flows, it can be said that the flow from the bottom channel is a necessary condition for the spanwise vortex such as the ones in Fig.28, Fig.29 and Fig.30.

Contour maps of Vz calculated with the measured data Vx and Vy in the lower measuring plane are shown in Fig.32 to Fig.36. Negative value is shown with dashed line and positive value is shown with solid line. As mentioned before, Vz value is the rough estimate and it may differs much from the true value in a strongly turbulent region. But looking at the whole flow field, there seems to be a flow pattern that corresponds to the spanwise vortex seen in the vector maps of the vertical measuring plane. The negative regions observed on the right side of the center line in Fig.33, Fig.34 and Fig.35 correspond to the downward flow seen in Fig.28, Fig.29 and Fig.30. The positive regions are generated on both sides of the negative region, and again there are negative regions near the inner wall. This pattern in Fig.34 and Fig.35 indicates that there are four vortices rotating vertically along the spanwise direction and there may be extra two vortices near the inner wall, in addition to the two vortices seen on the vector map of Fig.28 to Fig.30. Vz profile in Fig.36 also corresponds well to the vector map in Fig.31. Positive Vz is dominant in broad area on both sides of the center line and negative value exists near the side walls, which shows a pair of vortices.

The spanwise vortices are supposed to be generated by the combination of bottom channel and side channel flows. The flow from the bottom channel generates the stream directing to the upper wall of the main channel and the flow from the side channels generates the stream directing to the side walls at the upper part of the main channel, and the stream impinging to the side wall flows downward, which generates the spanwise vortex near the side wall, and this vortex induces the other vortex near the center line.

6. Conclusions

Using water as the model fluid, average flow behavior in the ESS target model was studied experimentally by UVP method for 3D structures.

The ESS target geometry has three inlet channels generating cross-flow on the surface of the target window, which was expected to prevent the creation of the recirculation region in the main channel or at least to reduce the effect. The results of the 3D mockup water experiments showed that the recirculation region is still generated on the reaction zone, at least, under the low flow rate conditions applied here. A pair of recirculations are observed on both sides of the center line of the model on the horizontal measuring plane.

When the flow rate ratio was 1:0:1, a large recirculation was generated covering the whole flow field, and when the bottom channel flow was introduced with the flow rate ratio of 2:1:2, the recirculation became small. As the bottom channel flow increased to the flow rate ratio of 1:2:1, the recirculation became larger and stronger. In accordance with this result, it might

be said that the bottom channel flow should be introduced with a small flow rate ratio in order to disturb and minimise the recirculation region. Increase of the flow rate ratio of the bottom channel will lead to the growth of the recirculation region.

Vector maps on the vertical measuring plane and Vz contour maps indicated that there are four counterrotating vortices in the spanwise direction. Those vortices may be induced by the combination of the bottom channel flow and the side channel flows, which generates the stream directing to the side wall at the upper part of the main channel. Since the shape of counterrotating vortices is clearer than in 2D model, they are considered to be intensified by the side channel flows, which makes the stream to the side wall stronger.

The recirculation region can be minimised by adjusting the flow rate ratio of inlet channels, but it may be difficult to vanish it or move it out of the spallation reaction zone with the present geometry. The shape and size of the vortices are supposed to be dependent on the model geometry and flow conditions of the target liquid, and it would be expected that different pattern of flow fields may appear with higher flow rates, but generally the large vortex structure seen with the low flow rate does not change even with higher flow rate. Together with continuing the experiment with the present ESS model, some modification should be considered including perforation of the side or bottom separation plate, and of course, numerical study with three dimensional model has to be done to decide the optimum target geometry and flow conditions.

Acknowledgements

The authors wish to thank Dr. Hiroshige Kikura for his helpful advice on this work and Mr. Filippo Barbagallo for the assistance and support for conducting the experiments.

References

[1] B.L.Smith, "Thermal Hydraulics of the ESS Liquid Metal Target" Proc. of ICANS-XIII and ESS-PM4, vol.2, pp577 (1995)

[2] Y. Takeda, T. Dury, and G.S. Bauer, "Liquid metal target for spallation neutron sources" Proc. of NURETH-8, Vol.2, pp1252 (1997)

[3] Y. Takeda, Velocity profile measurement by ultrasonic Doppler method, Exp. Therm. & Fluid Sci., 10, 444-453, (1995)

[4] Y.Takeda, Ed., First International Symposium on Ultrasonic Doppler Methods for Fluid Mechanics and Fluid Engineering, PSI, Switzerland, 9.-11. Sept., 1996

[5] H. Kikura & Y. Takeda, ASME Fluid Engineering Division, Summer Meeting, Washington DC, July 98

Table 1 Flow Rate Conditions for the Water Experiments of the ESS Target Model

Data-Set Nr.	MP Height [mm]	MP Angle [deg]	Flow Rate [L / s]				Flow Velocity at the Front Edge [mm/s]			ML Set Nr.
			A	B	C	Total	A	B	C	
1	0	0	0.33	0.33	0.33	0.99	456	413	456	1
2	0	0	0.33	0.33	0.33	0.99	456	413	456	2
3	0	0	0.33	0.33	0.33	0.99	456	413	456	3
4	0	0	0.33	0.33	0.33	0.99	456	413	456	4
5	0	0	0.33	0.66	0.33	1.32	456	825	456	5
6	0	0	0.22	0.22	0.22	0.66	304	275	304	6
7	0	0	0.22	0.44	0.22	0.88	304	550	304	7
8	0	0	0.44	0	0.44	0.88	608	0	608	7
9	0	0	0.35	0.18	0.35	0.88	483	225	483	7
10	0	0	0	0.88	0	0.88	0	1100	0	7
11	0	0	0.29	0.29	0.29	0.88	401	363	401	7
12	+10	0	0.22	0.44	0.22	0.88	304	550	304	7
13	+10	0	0.44	0	0.44	0.88	608	0	608	7
14	+10	0	0.35	0.18	0.35	0.88	483	225	483	7
15	+10	0	0.29	0.29	0.29	0.88	401	363	401	7
16	+10	0	0	0.88	0	0.88	0	1100	0	7
17	-10	0	0.22	0.44	0.22	0.88	304	550	304	7
18	-10	0	0.29	0.29	0.29	0.88	401	363	401	7
19	-10	0	0.44	0	0.44	0.88	608	0	608	7
20	-10	0	0.35	0.18	0.35	0.88	483	225	483	7
21	-10	0	0	0.88	0	0.88	0	1100	0	7
22	-20	+10	0.29	0.29	0.29	0.88	401	363	401	7
23	-20	+10	0.44	0	0.44	0.88	608	0	608	8
24	-20	+10	0.22	0.44	0.22	0.88	304	550	304	8
25	-20	+10	0.35	0.18	0.35	0.88	483	225	483	8
26	-20	+10	0	0.88	0	0.88	0	1100	0	8
27	-	-85	0	0.88	0	0.88	0	1100	0	9
28	-	-85	0.44	0	0.44	0.88	608	0	608	9
29	-	-85	0.29	0.29	0.29	0.88	401	363	401	9
30	-	-85	0.22	0.44	0.22	0.88	304	550	304	9
31	-	-85	0.35	0.18	0.35	0.88	483	225	483	9

MP : Measuring Plane ML : Measuring Line

Table 2 Figure Number for Each Experimental condition

MP Angle [°]	MP Height [mm]	Flow Rate Ratio (A : B : C)				
		1:0:1	2:1:2	1:1:1	1:2:1	0:1:0
0 (Horizontal)	+10	Fig.7 [13]	Fig.8 [14]	Fig.9 [15]	Fig.10 [12]	Fig.11 [16]
	0	Fig.12 [8]	Fig.13 [9]	Fig.14 [11]	Fig.15 [7]	Fig.16 [10]
	-10	Fig.17 [19]	Fig.18 [20]	Fig.19 [18]	Fig.20 [17]	Fig.21 [21]
+10 (Slant)	-20	Fig.22 [23]	Fig.23 [25]	Fig.24 [22]	Fig.25 [24]	Fig.26 [26]
-85 (Vertical)	-	Fig.27 [28]	Fig.28 [31]	Fig.29 [29]	Fig.30 [30]	Fig.31 [27]

[ ] : Data Set Number

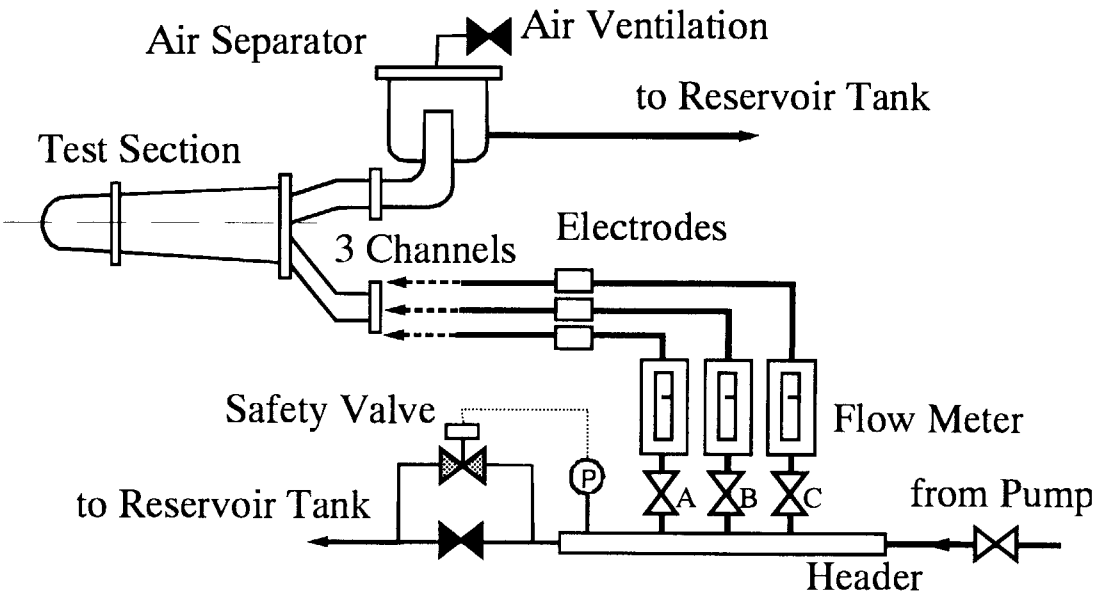

Fig.1 Water Loop for ESS Experiment

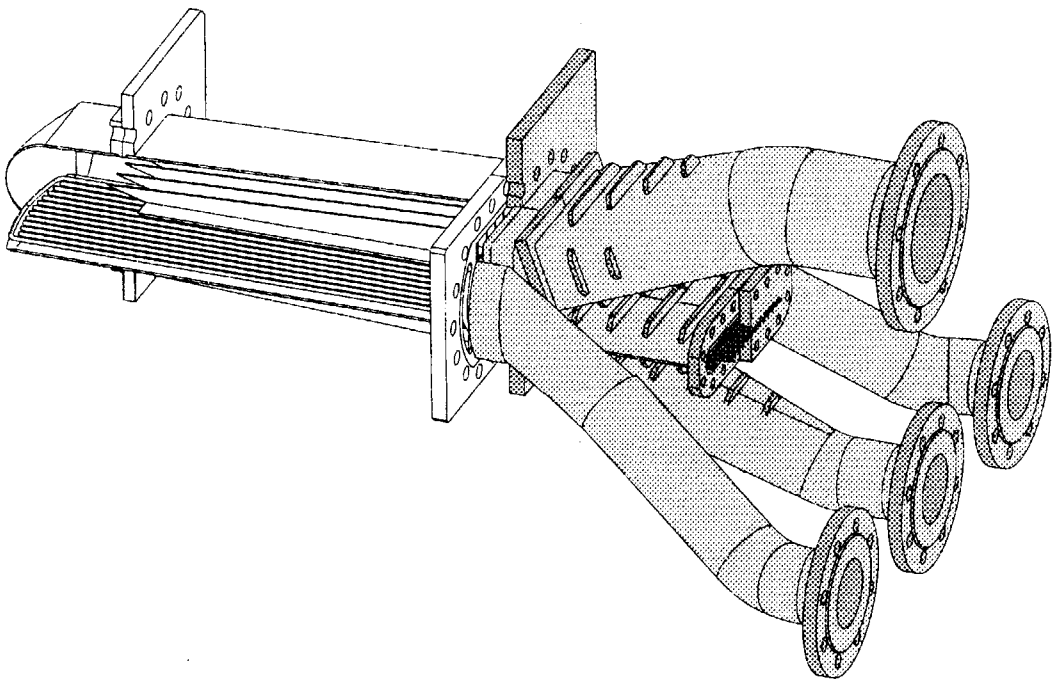

Fig.2 Cut-out View of the ESS Model

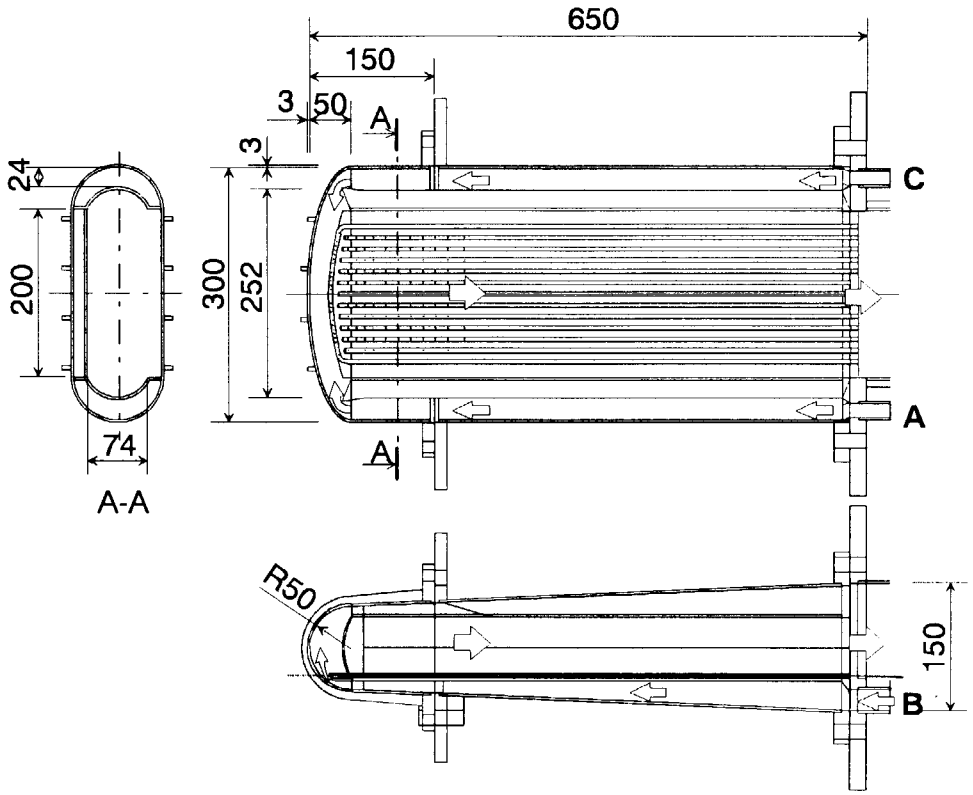

Fig.3 Dimensions of the Target Model

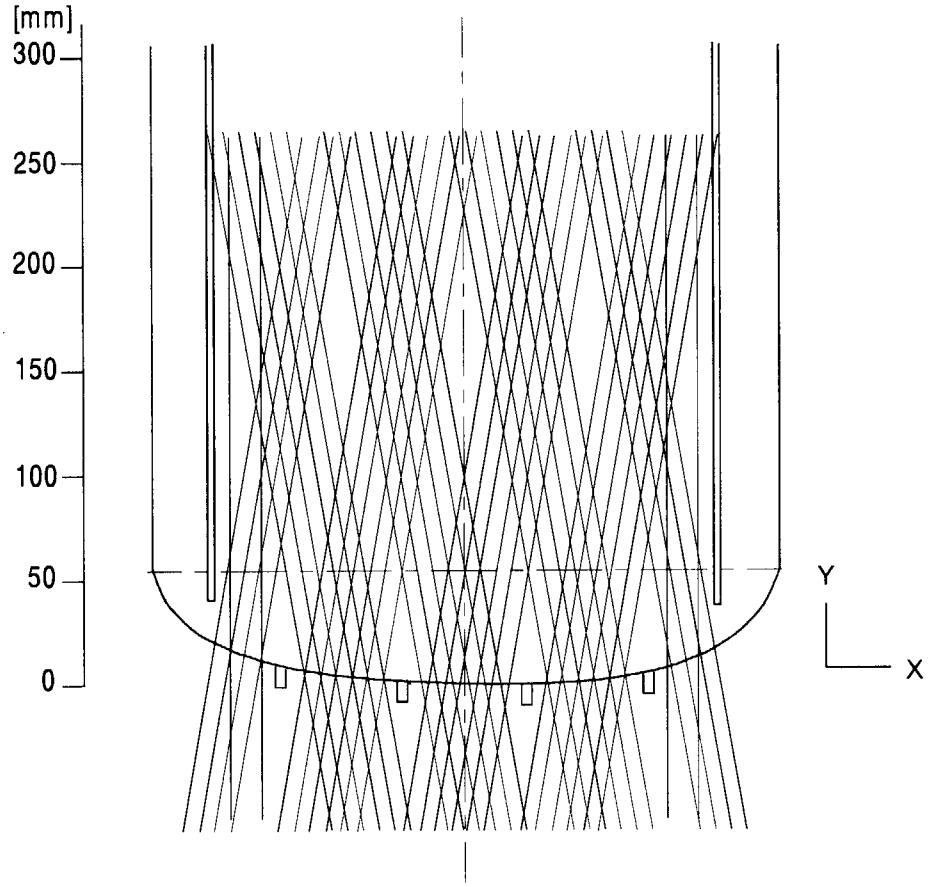

Fig.4 Arrangement of Measuring Lines on the Horizontal Plane

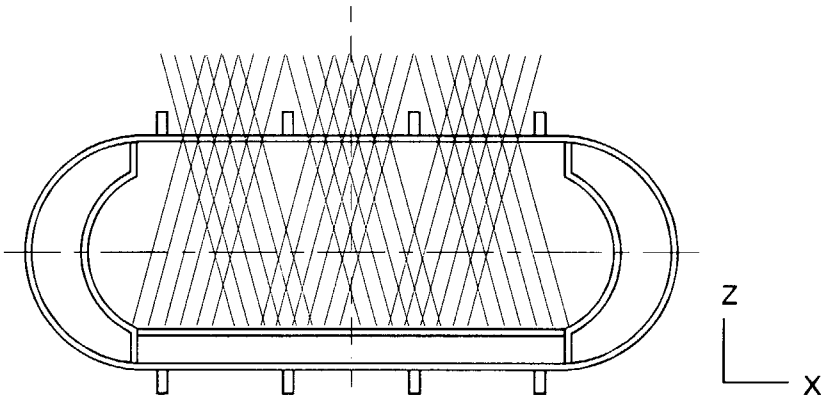

Fig.5 Arrangement of Measuring Lines on the Vertical Plane

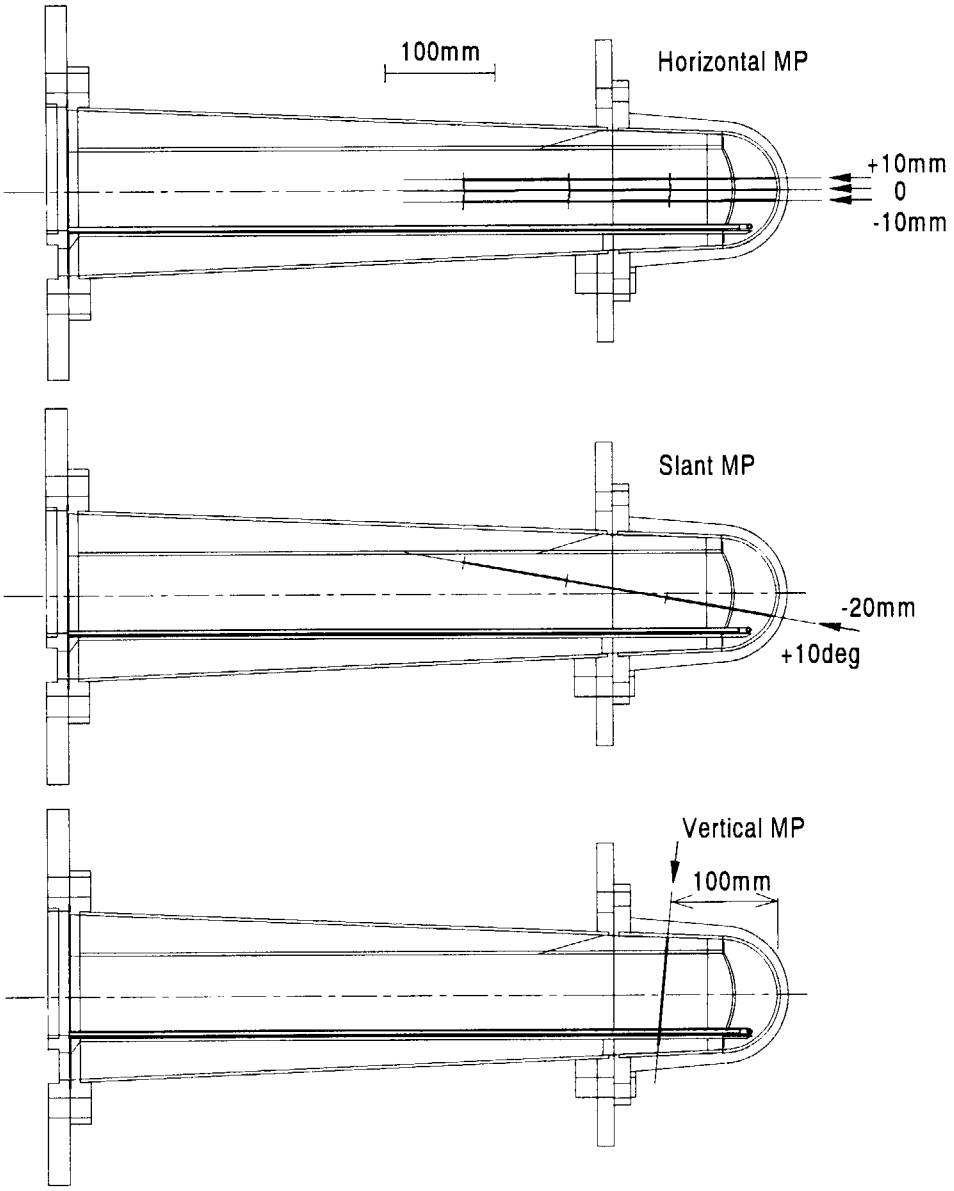

Fig.6 Position of Measuring Planes

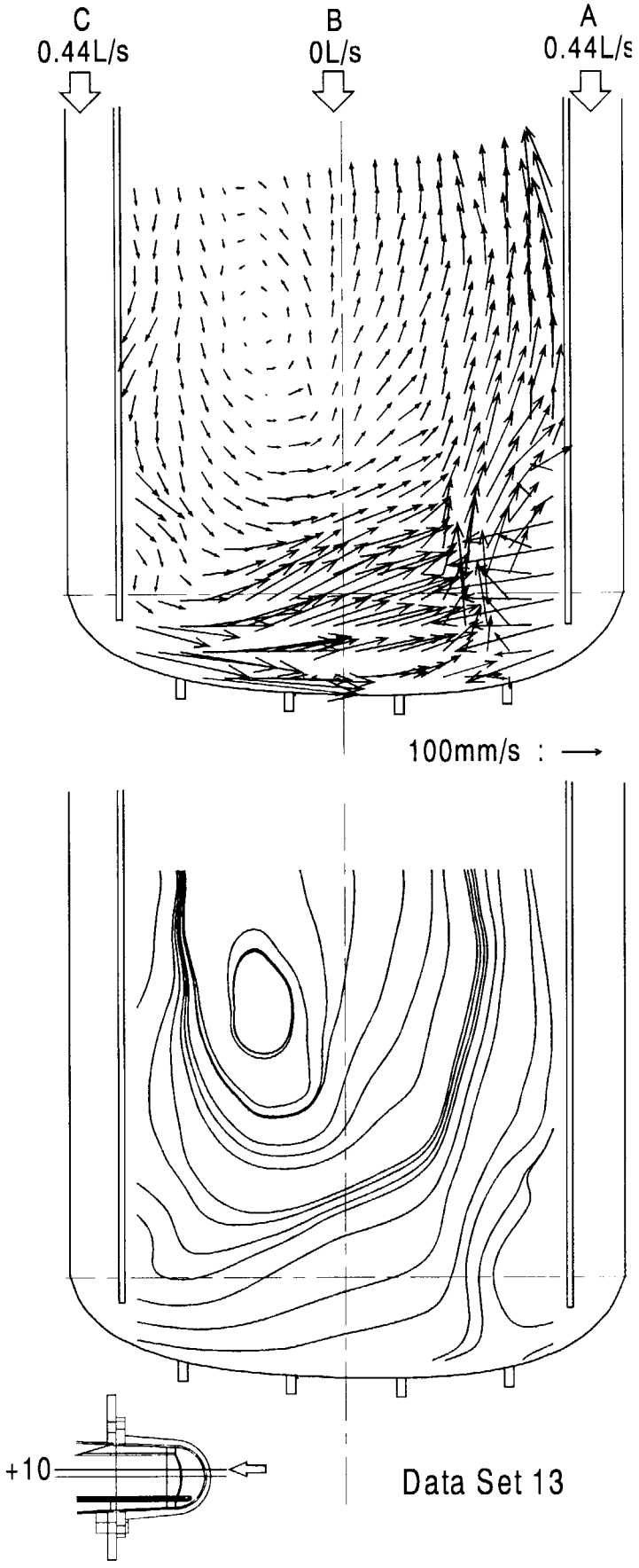

Fig.7 Flow Field in the ESS Model (1 : 0 : 1)

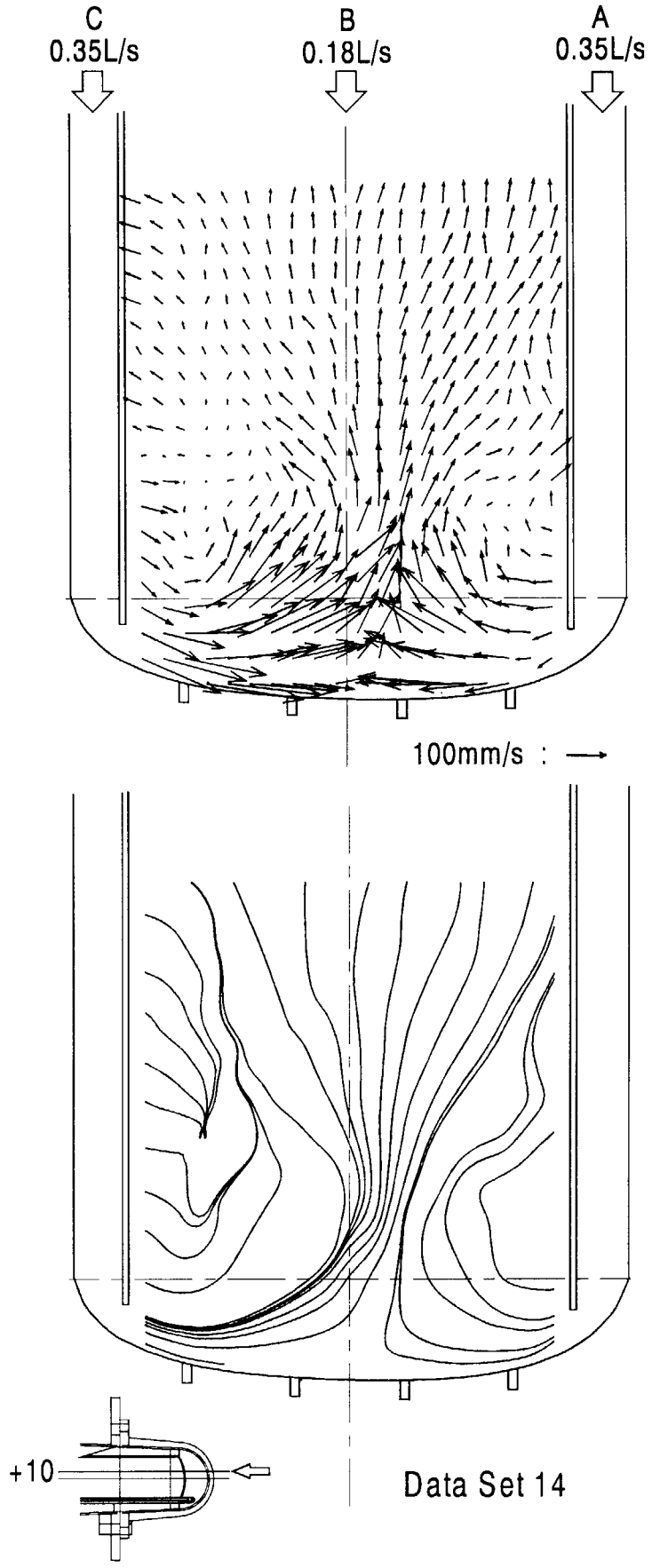

Fig.8 Flow Field in the ESS Model (2 : 1 : 2)

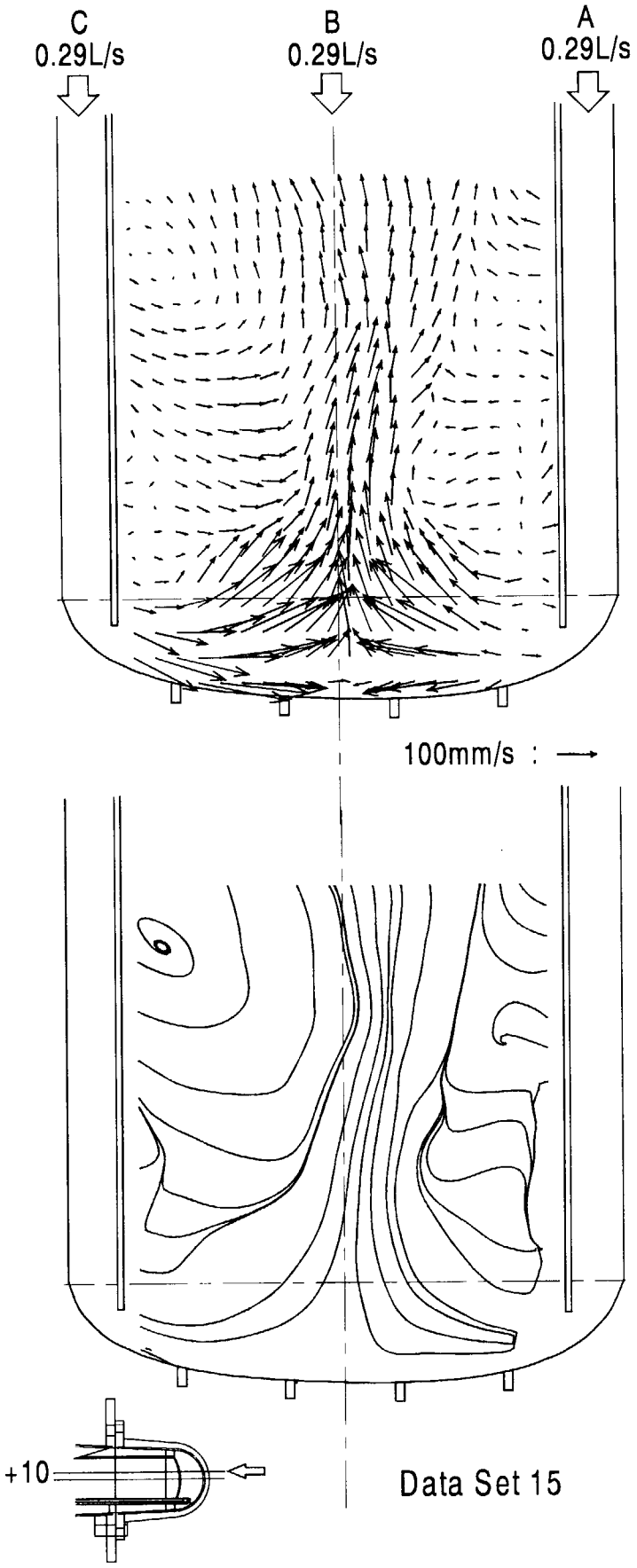

Fig.9 Flow Field in the ESS Model (1 : 1 : 1)

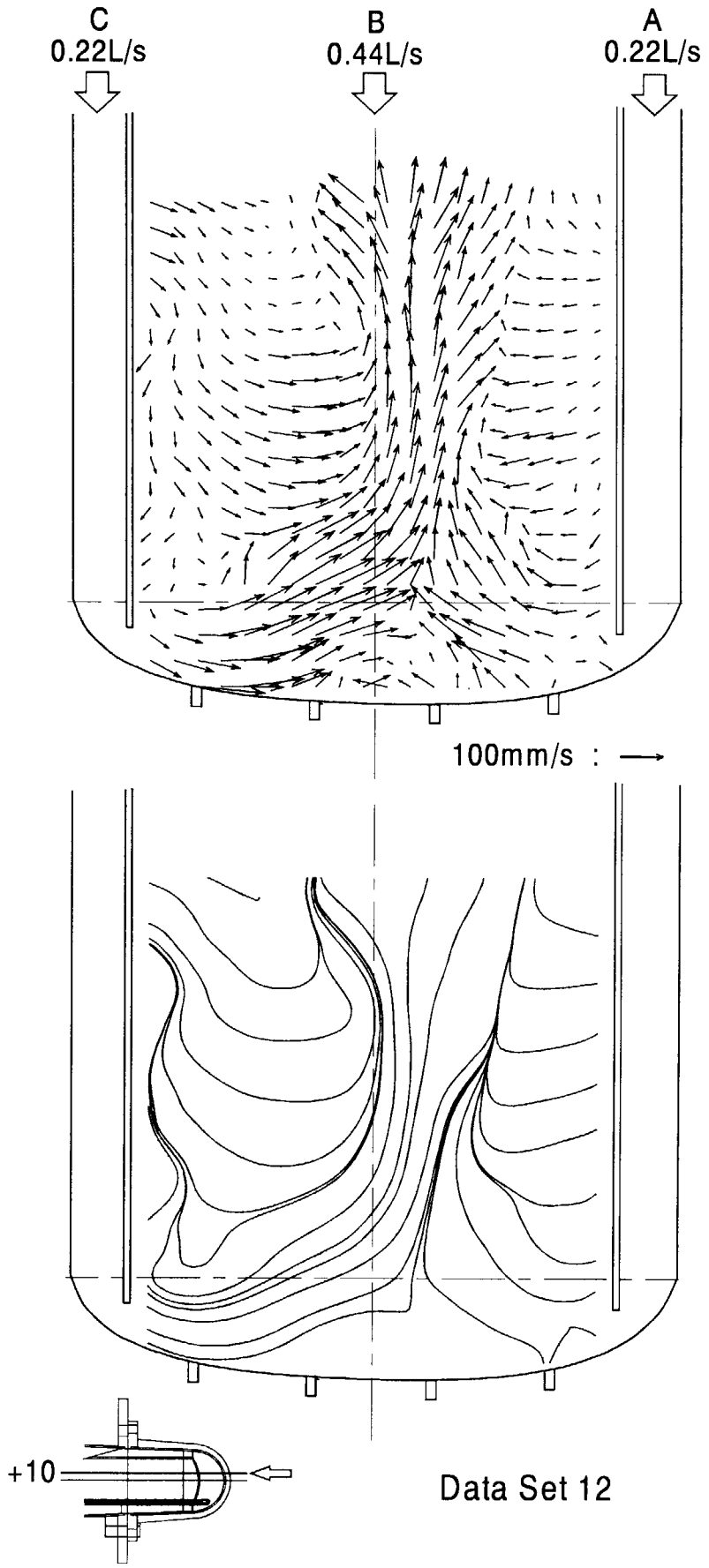

Fig.10 Flow Field in the ESS Model (1 : 2 : 1)

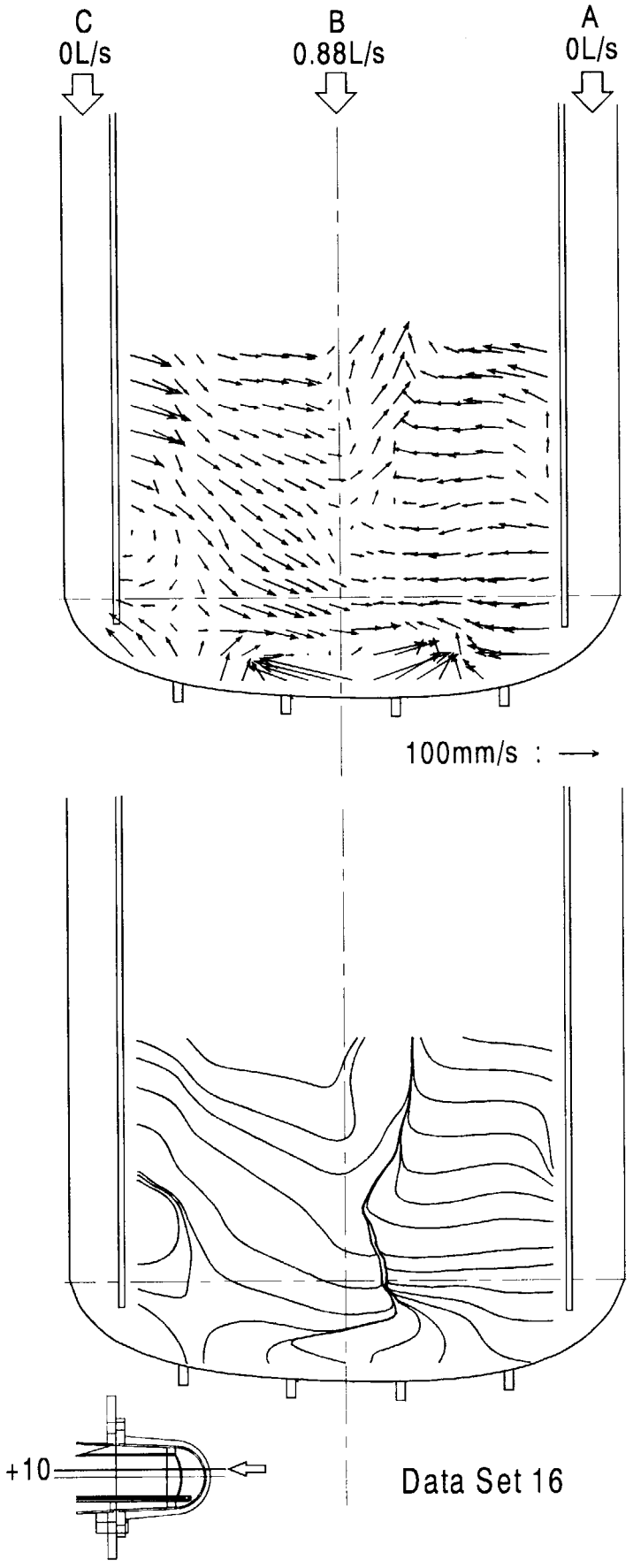

Fig.11 Flow Field in the ESS Model (0 : 1 : 0)

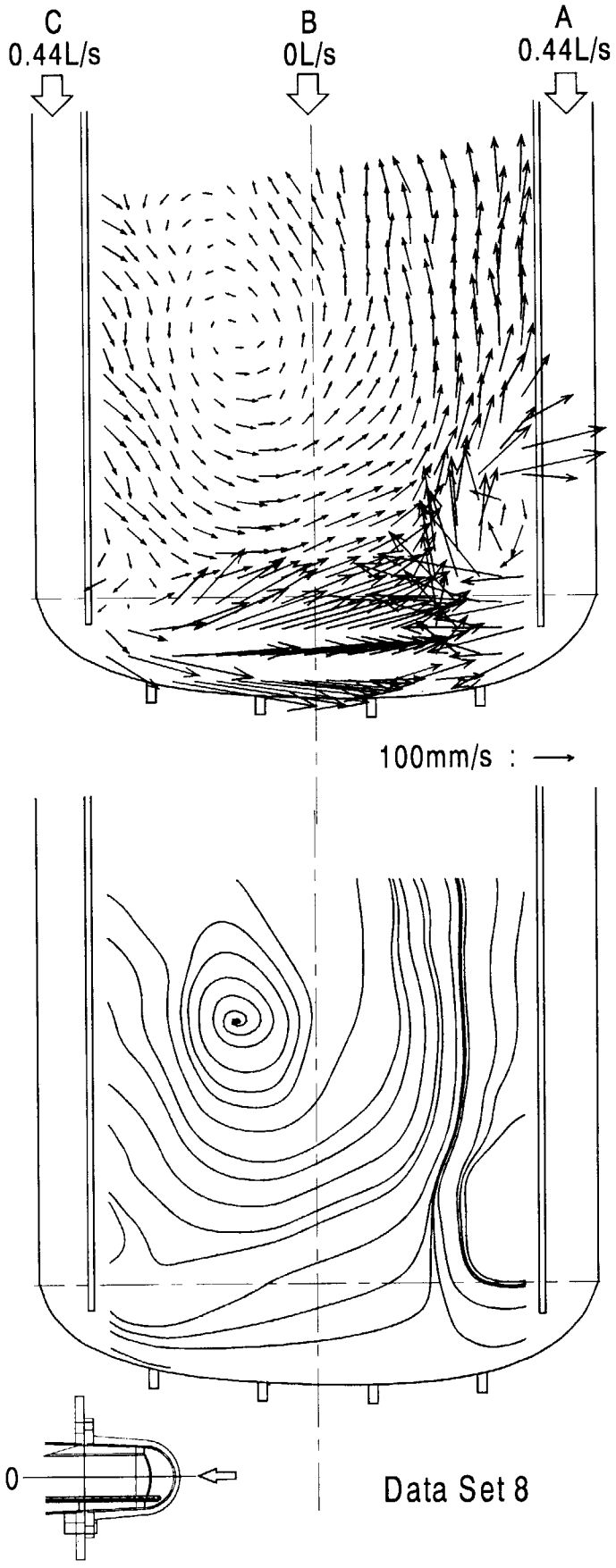

Fig.12 Flow Field in the ESS Model (1 : 0 : 1)

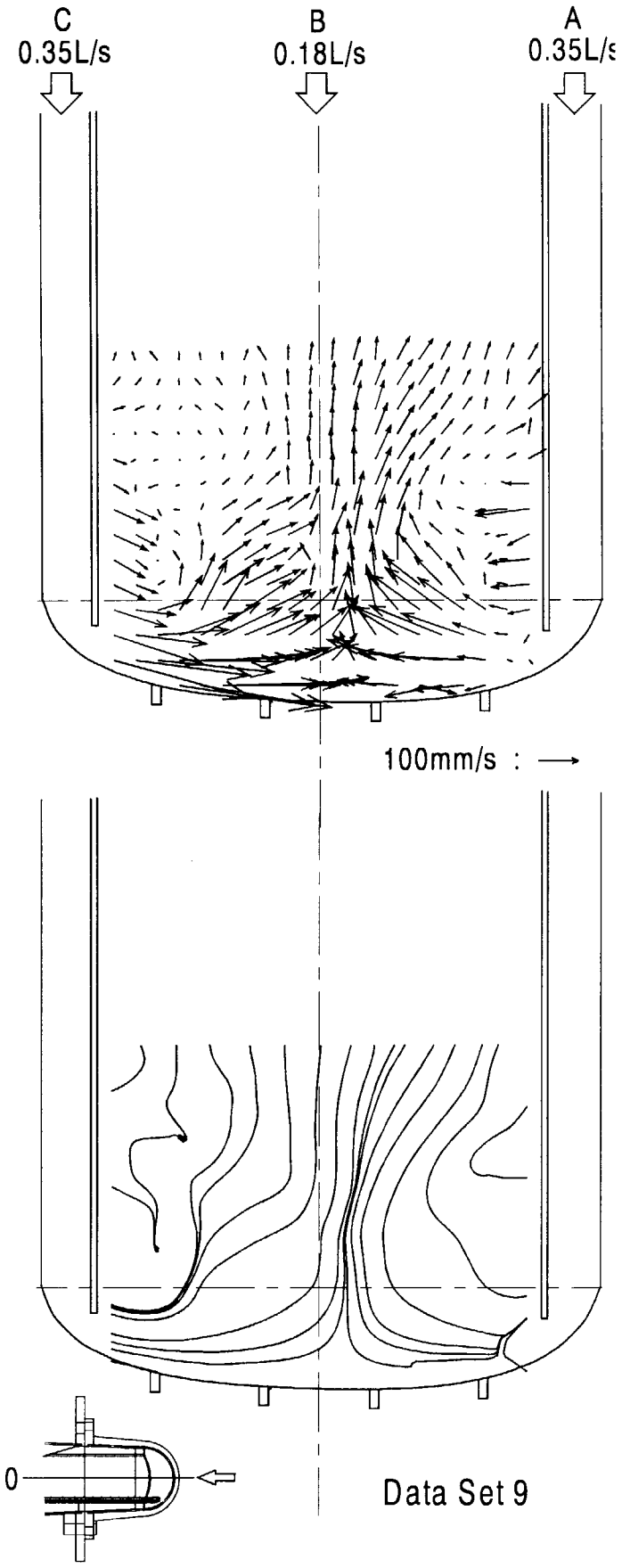

Fig.13 Flow Field in the ESS Model (2 : 1 : 2)

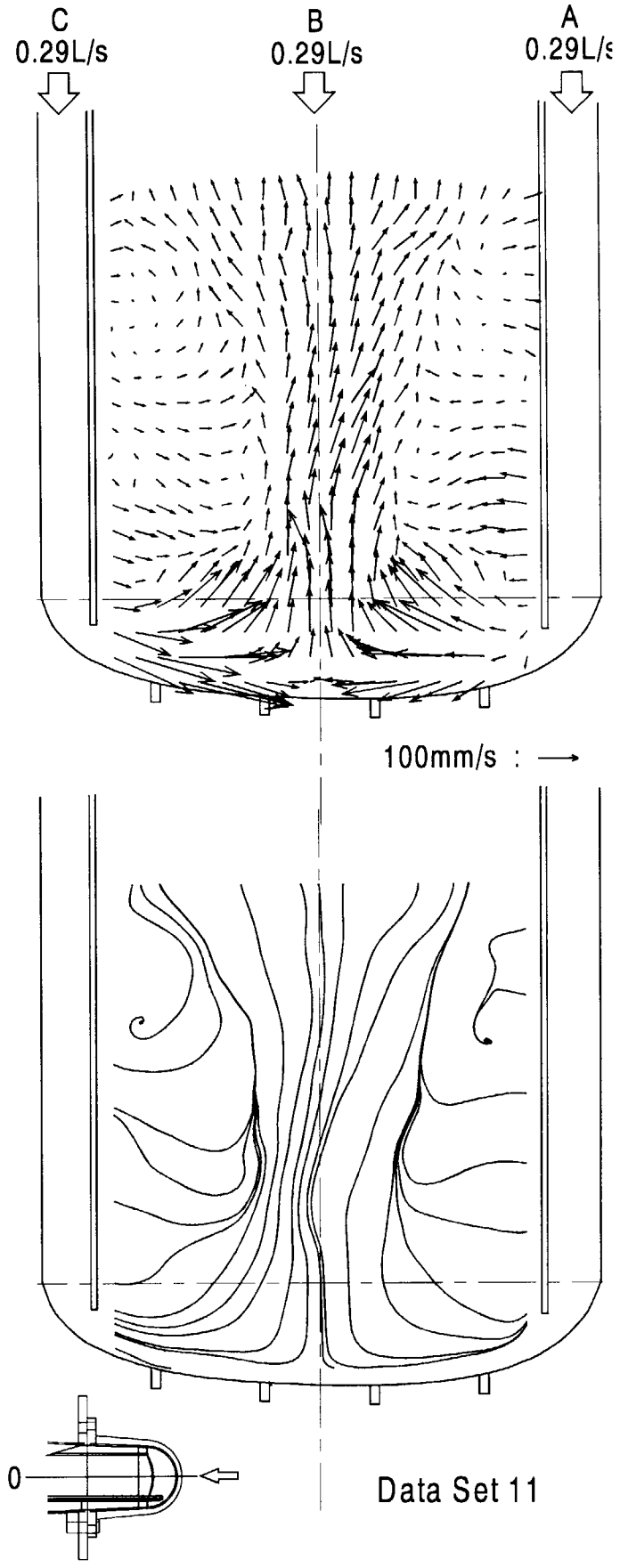

Fig.14 Flow Field in the ESS Model (1 : 1 : 1)

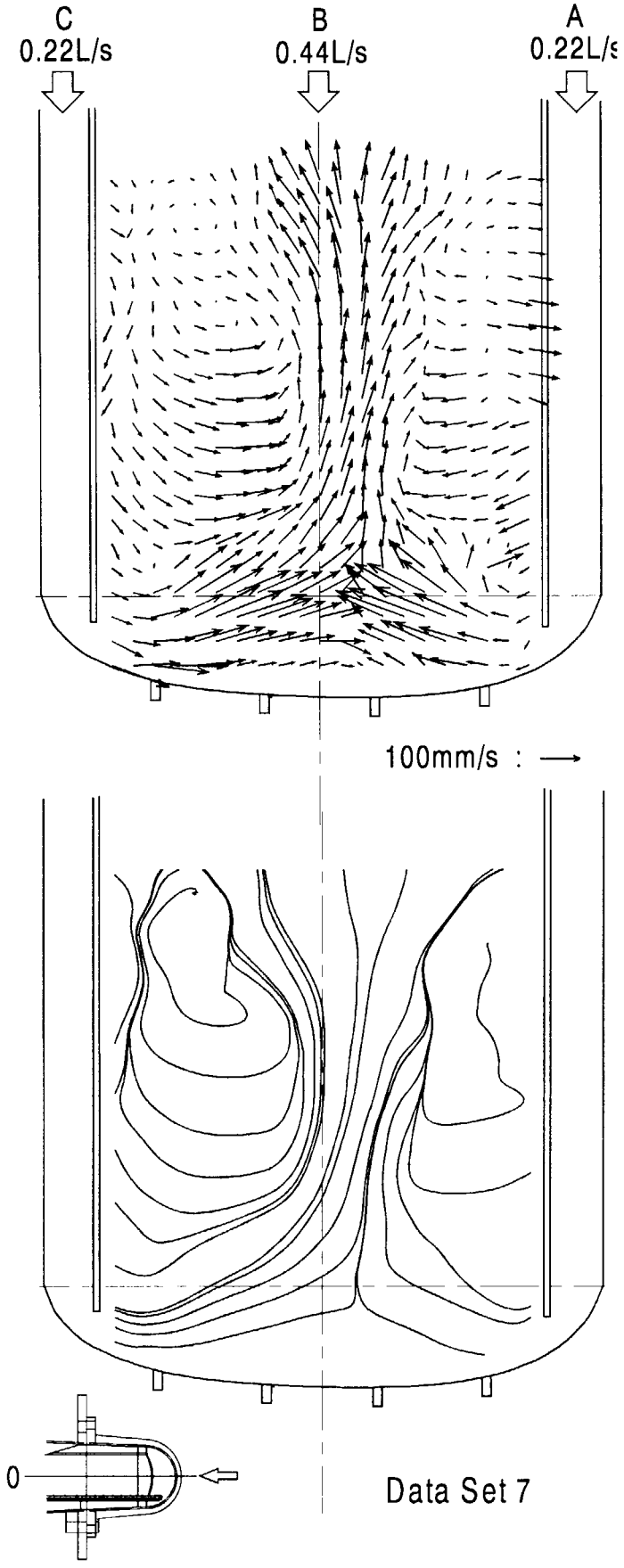

Fig.15 Flow Field in the ESS Model (1 : 2 : 1)

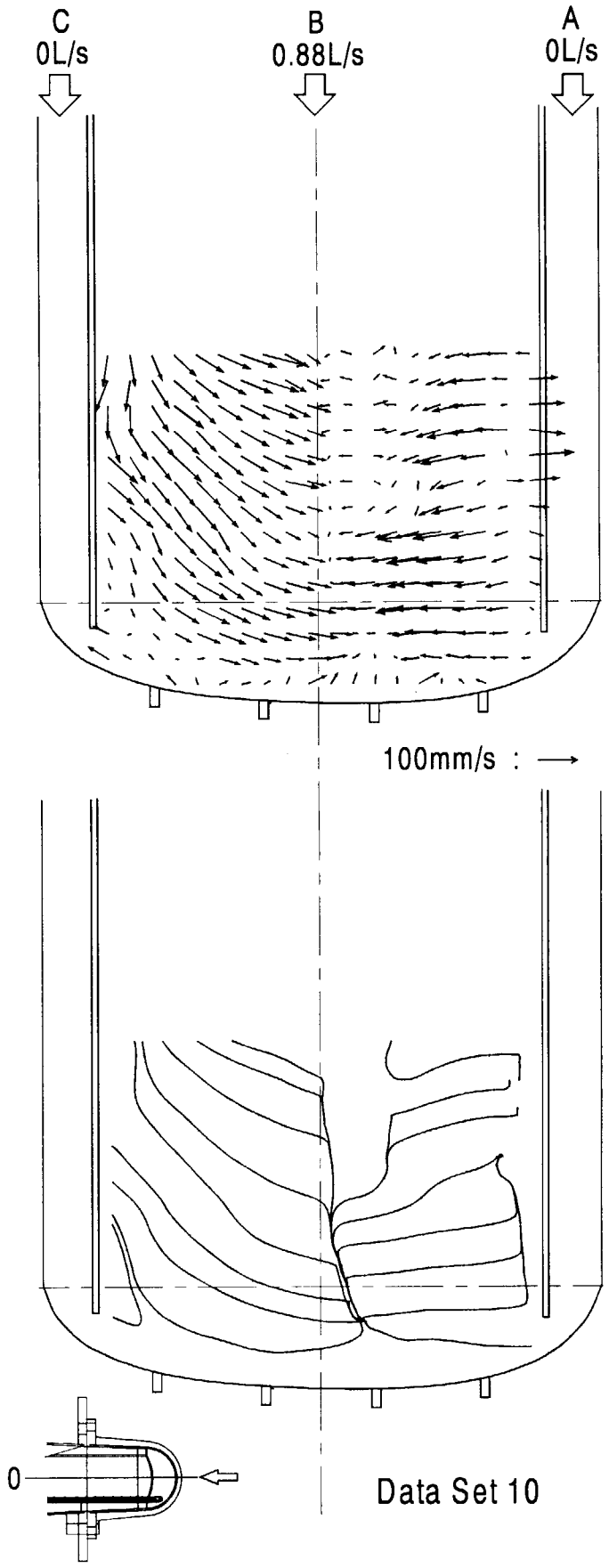

Fig.16 Flow Field in the ESS Model (0 : 1 : 0)

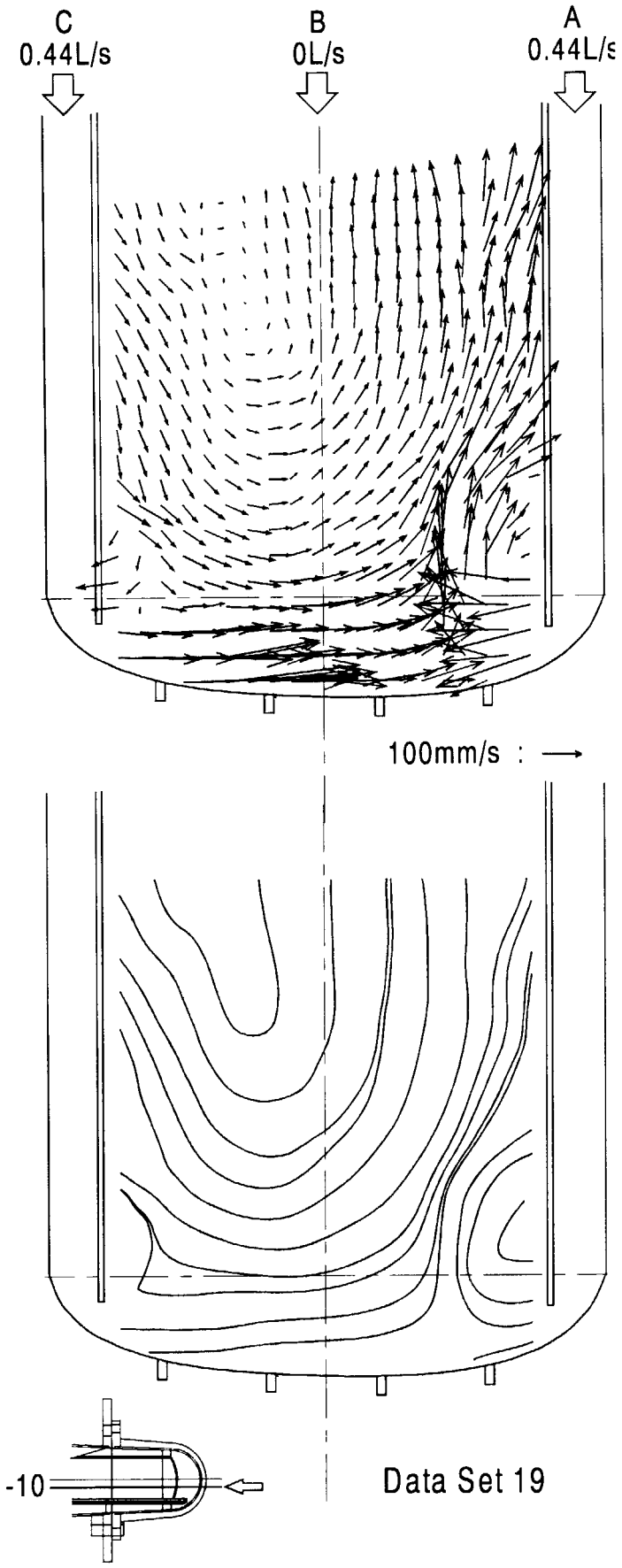

Fig.17 Flow Field in the ESS Model (1 : 0 : 1)

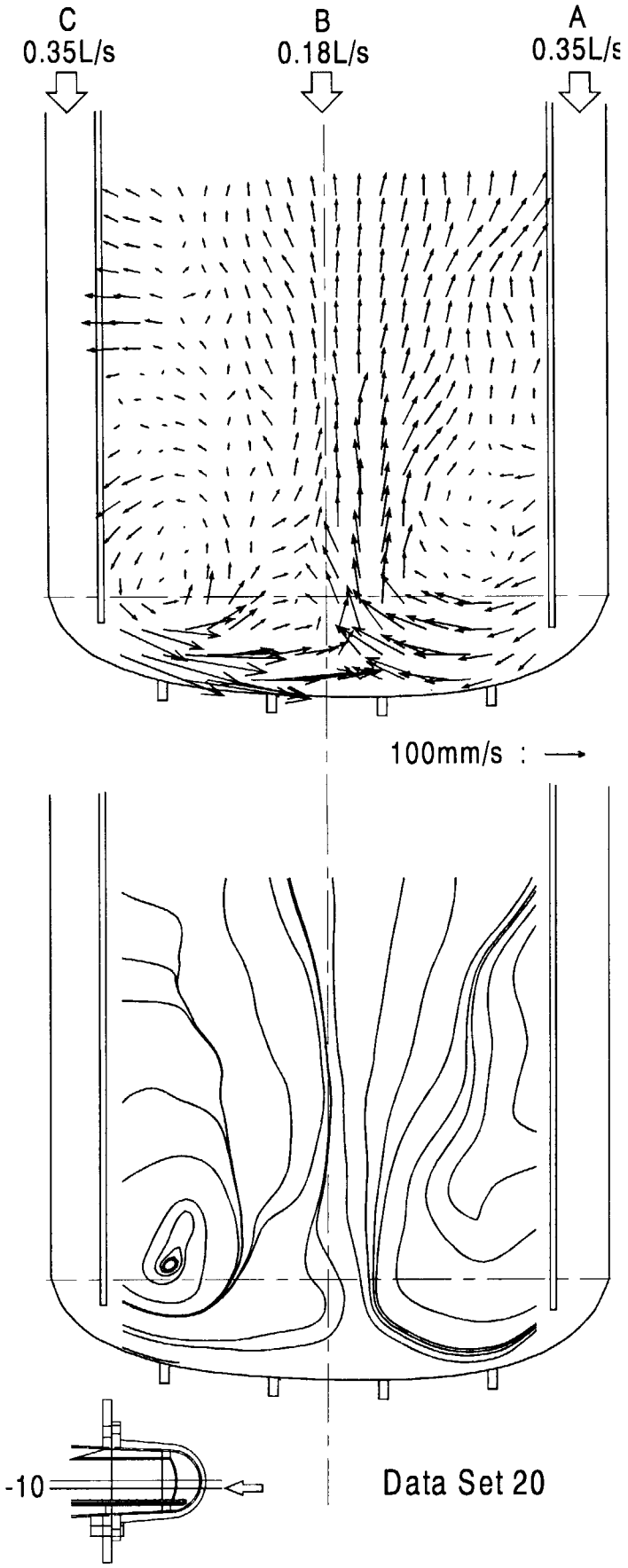

Fig.18 Flow Field in the ESS Model (2 : 1 : 2)

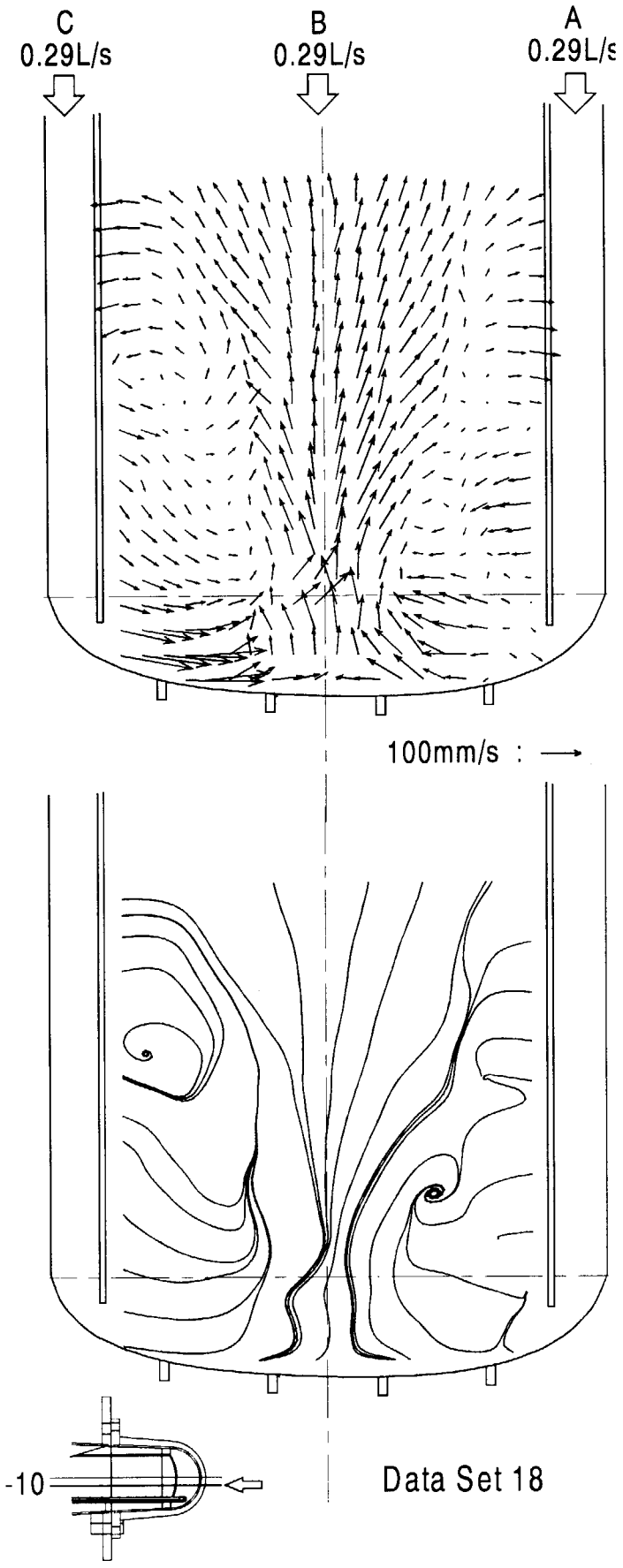

Fig.19 Flow Field in the ESS Model (1 : 1 : 1)

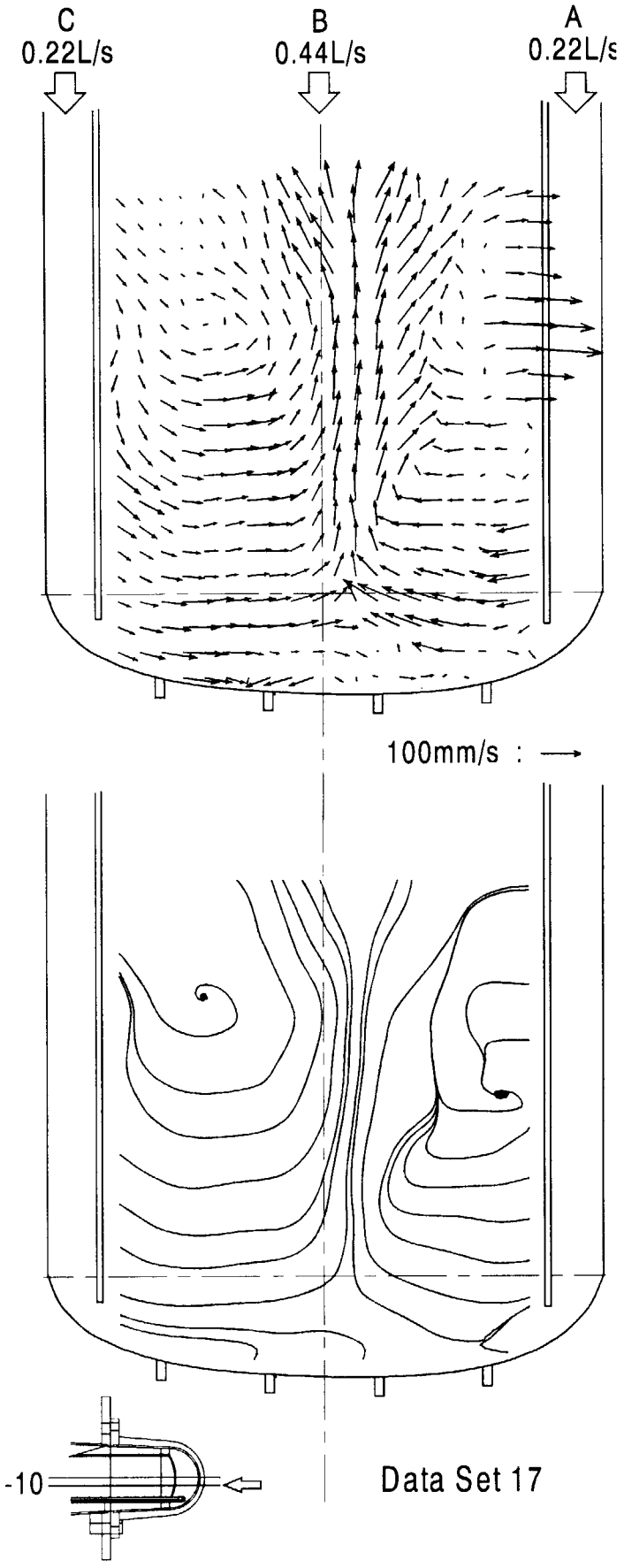

Fig.20 Flow Field in the ESS Model (1 : 2 : 1)

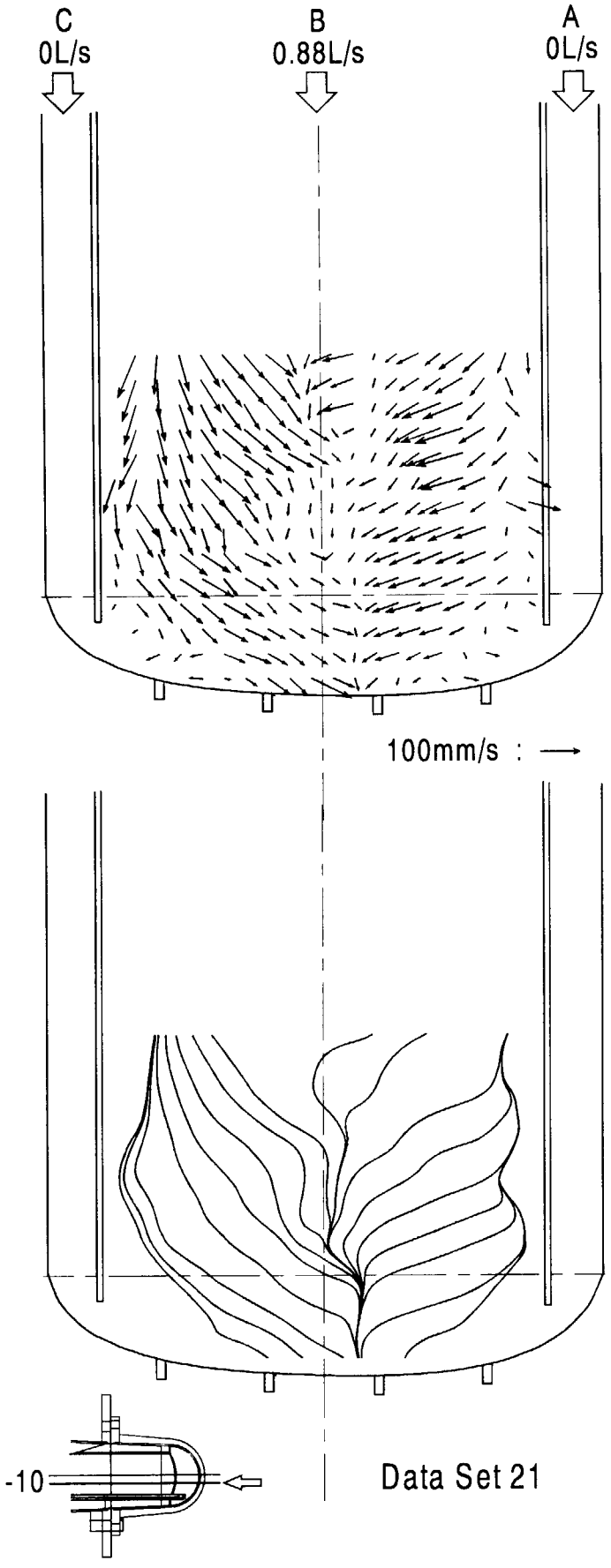

Fig.21 Flow Field in the ESS Model (0 : 1 : 0)

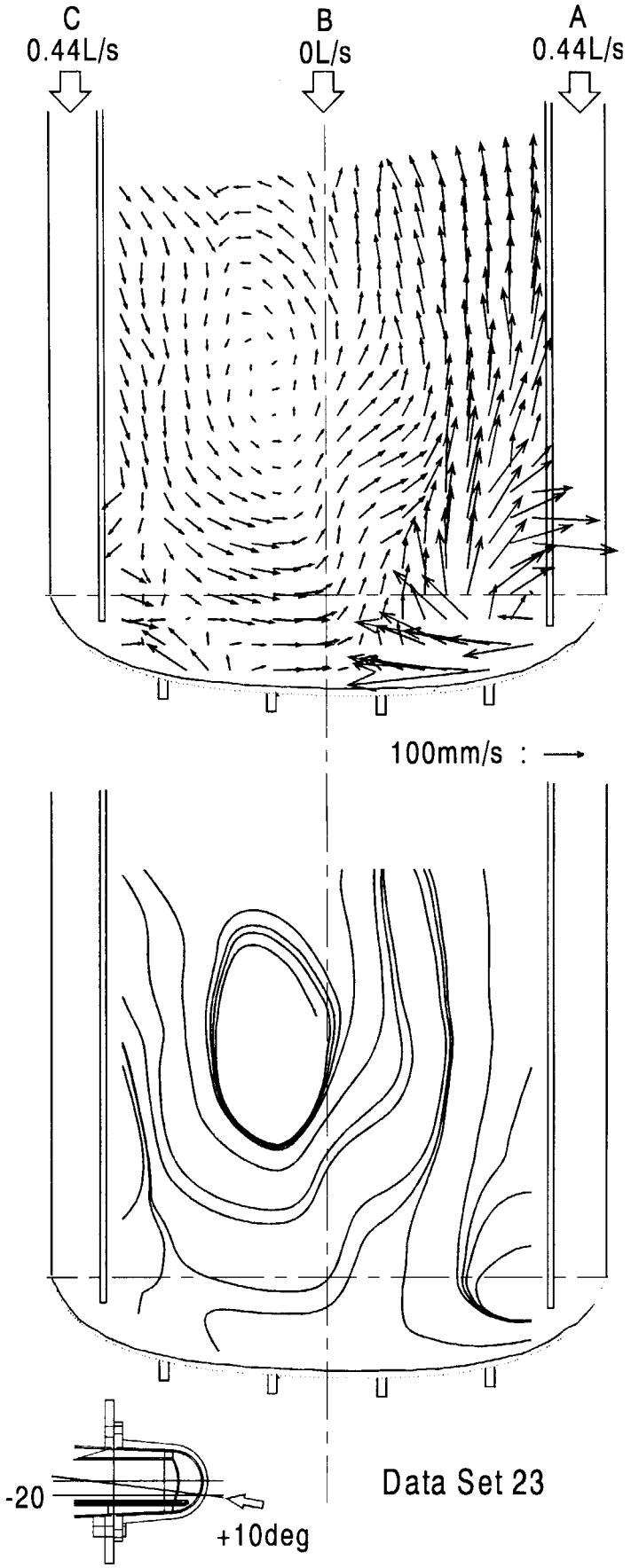

Fig.22 Flow Field in the ESS Model (1 : 0 : 1)

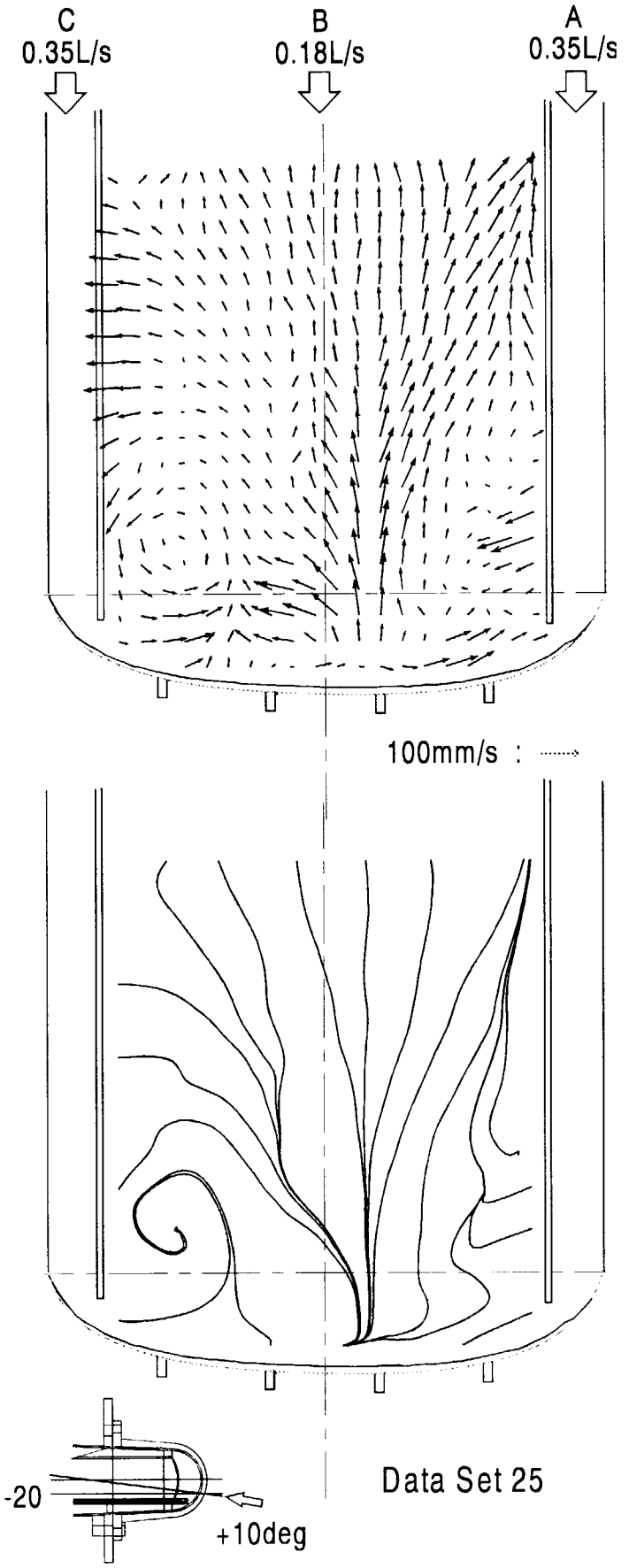

Fig.23 Flow Field in the ESS Model (2 : 1 : 2)

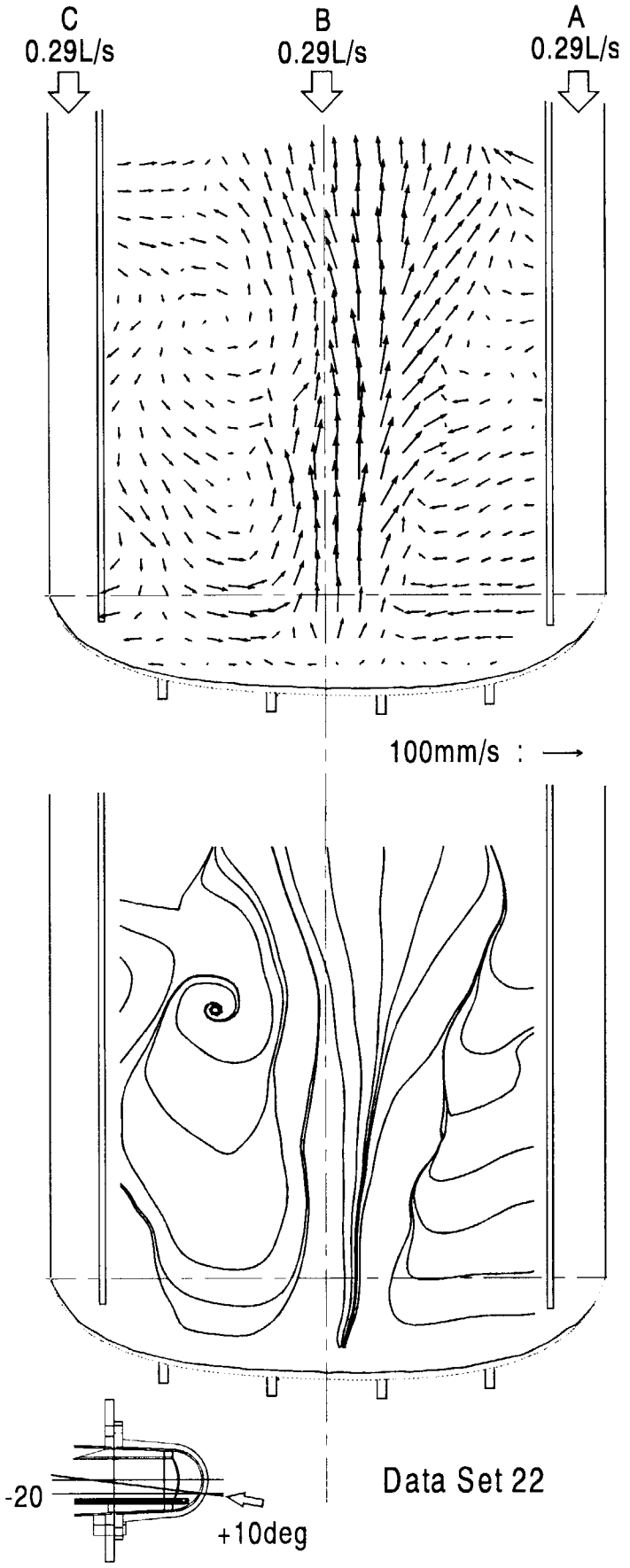

Fig.24 Flow Field in the ESS Model (1 : 1 : 1)

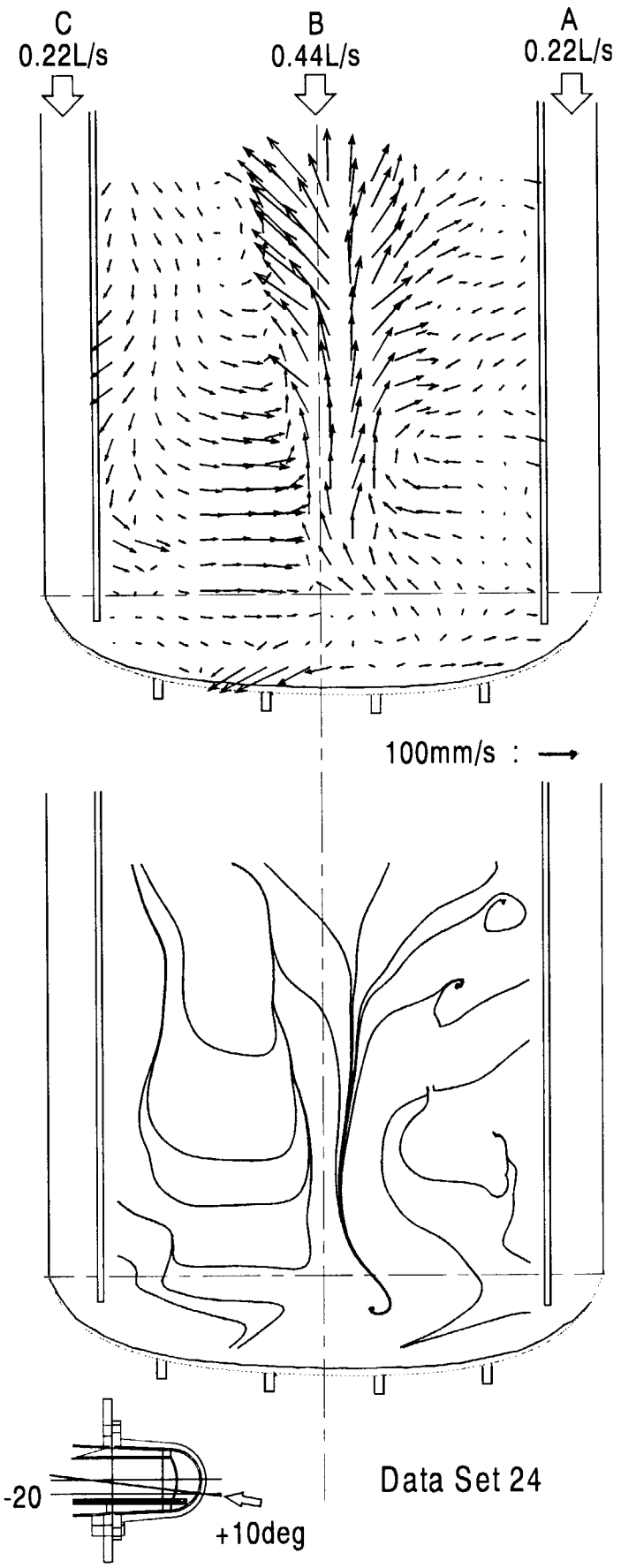

Fig.25 Flow Field in the ESS Model (1 : 2 : 1)

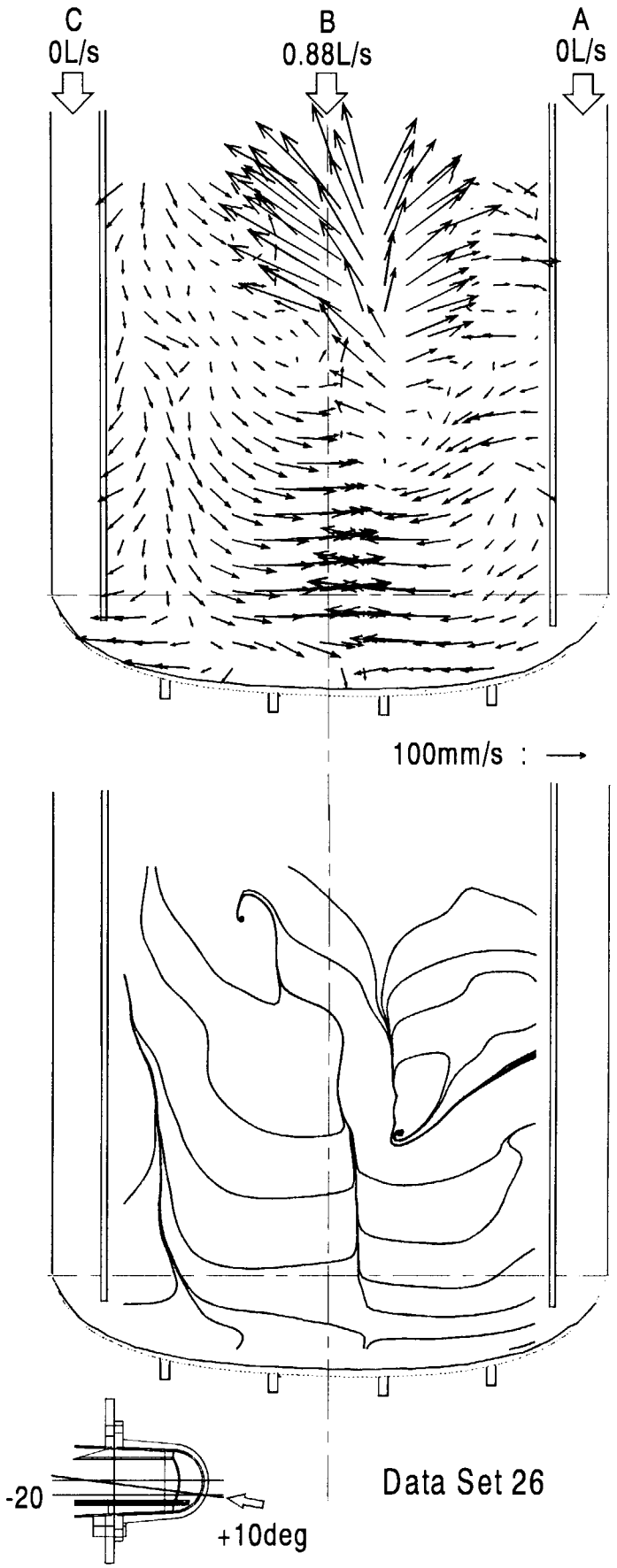

Fig.26 Flow Field in the ESS Model (0 : 1 : 0)

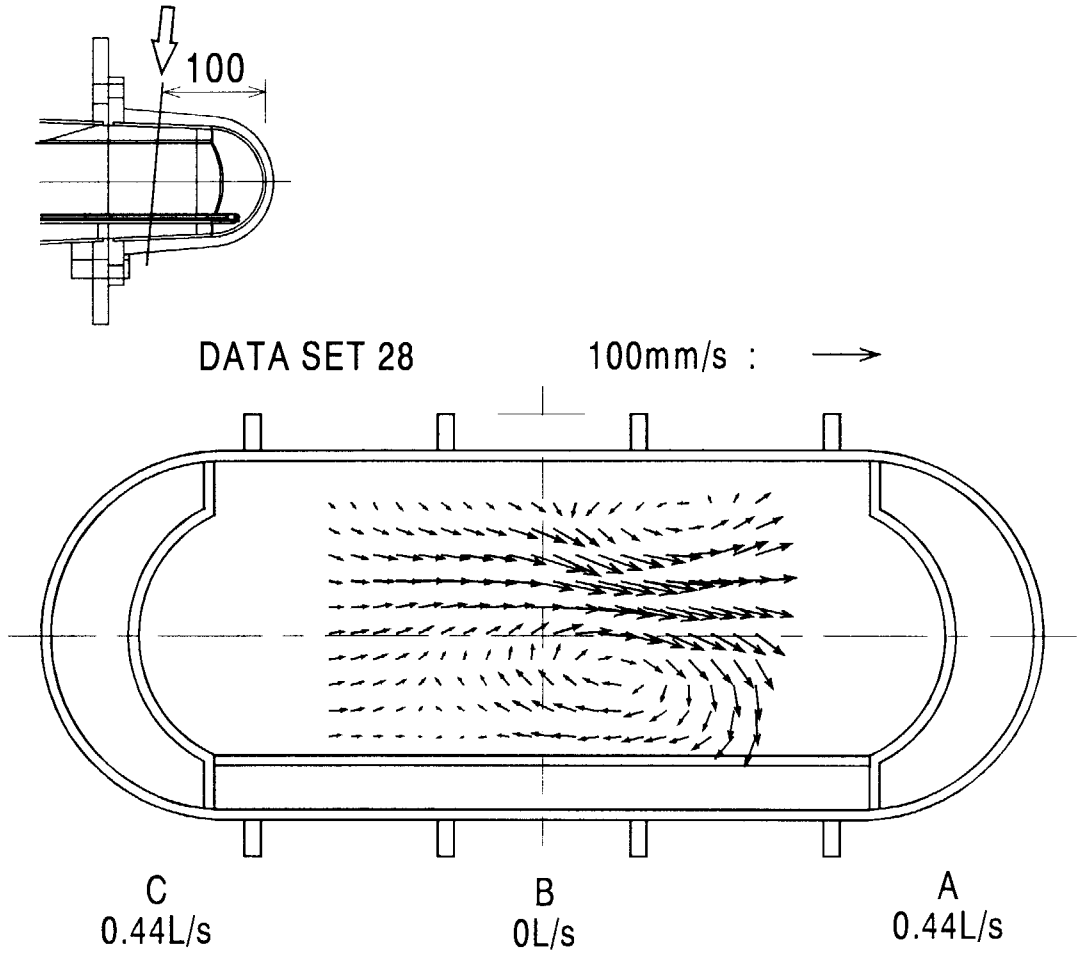

Fig.27 Vector Flow Field (1 : 0 : 1)

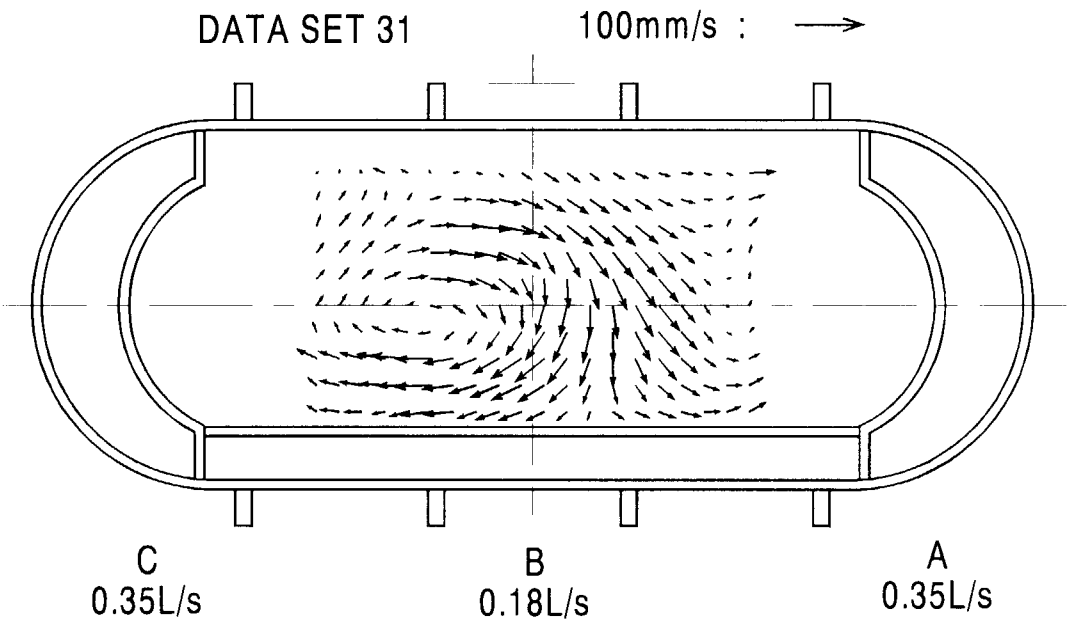

Fig.28 Vector Flow Field (2 : 1 : 2)

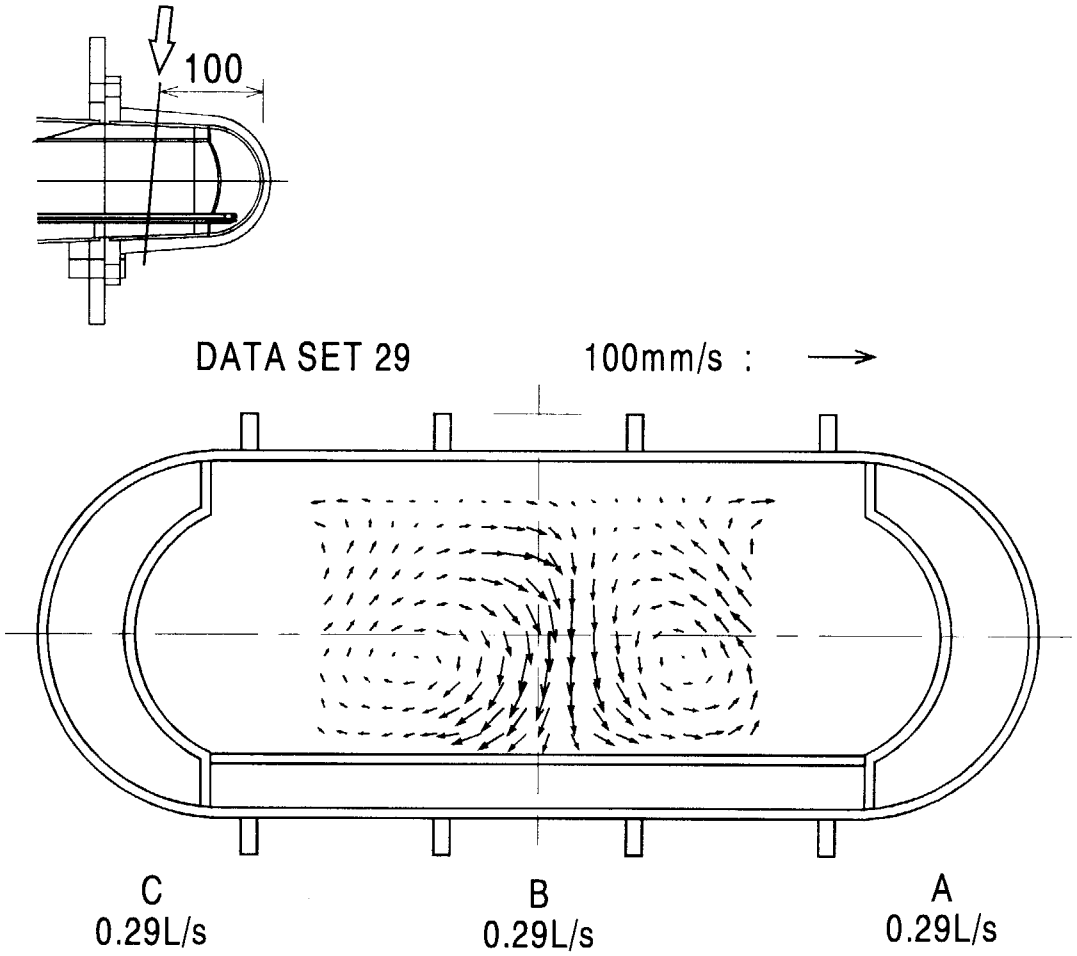

Fig.29 Vector Flow Field (1 : 1 : 1)

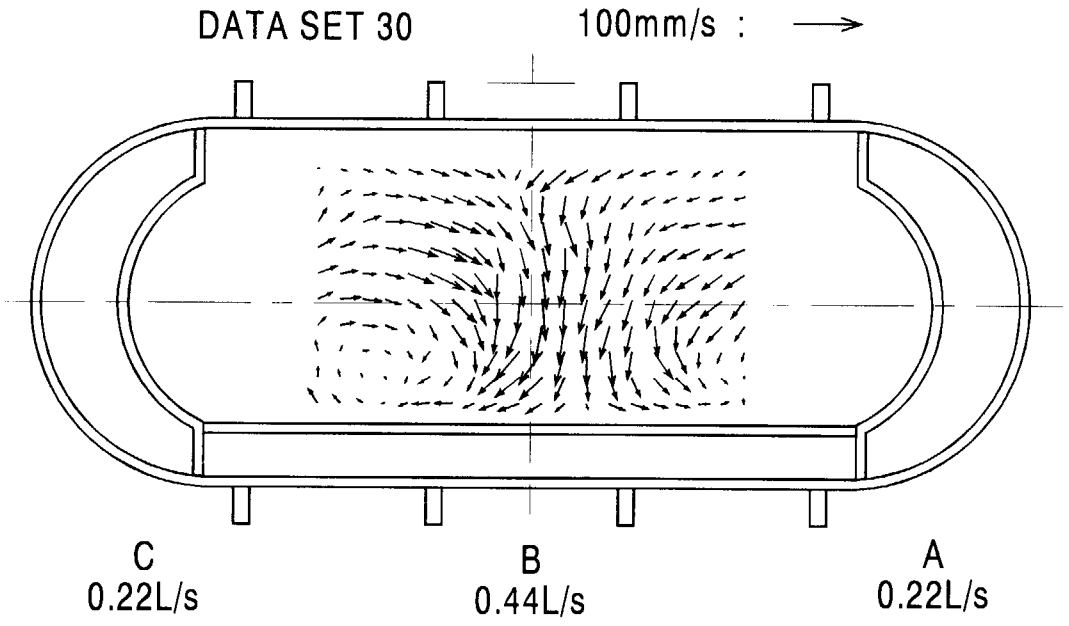

Fig.30 Vector Flow Field (1 : 2 : 1)

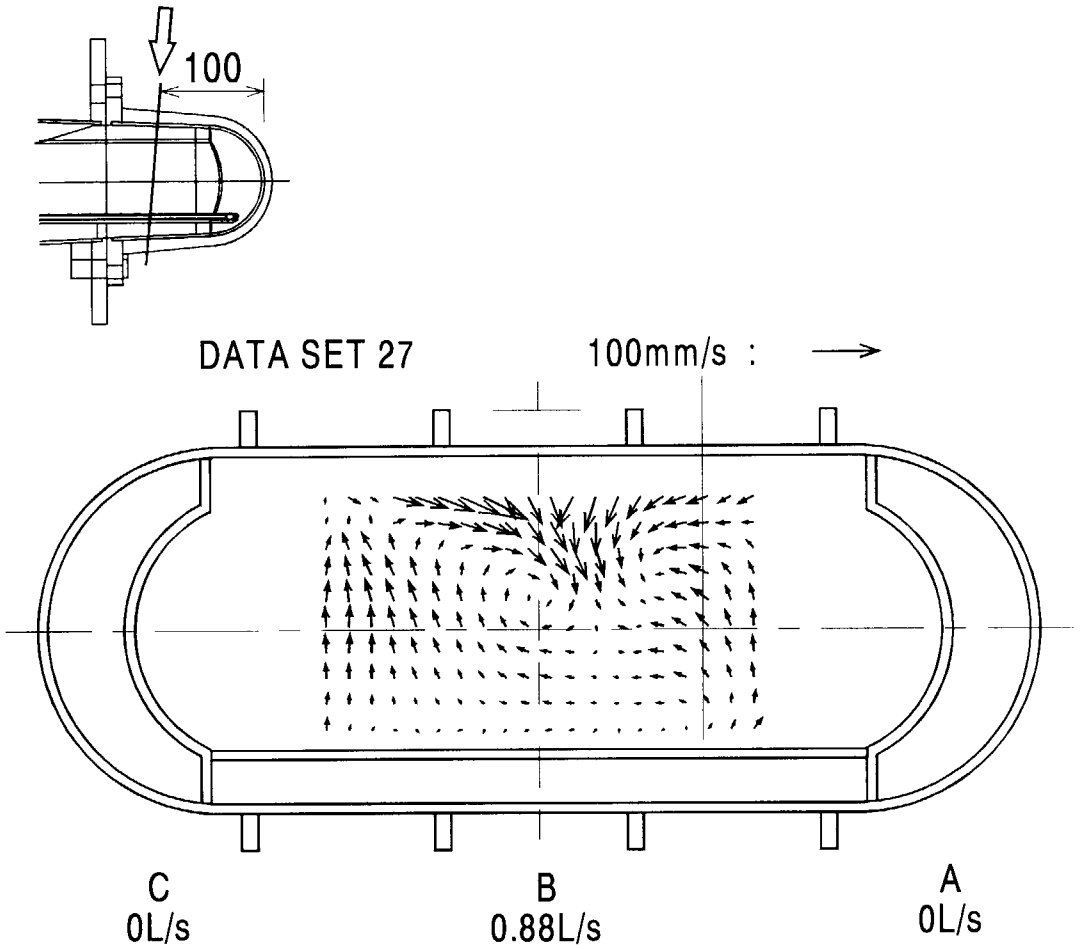

Fig.31 Vector Flow Field (0 : 1 : 0)

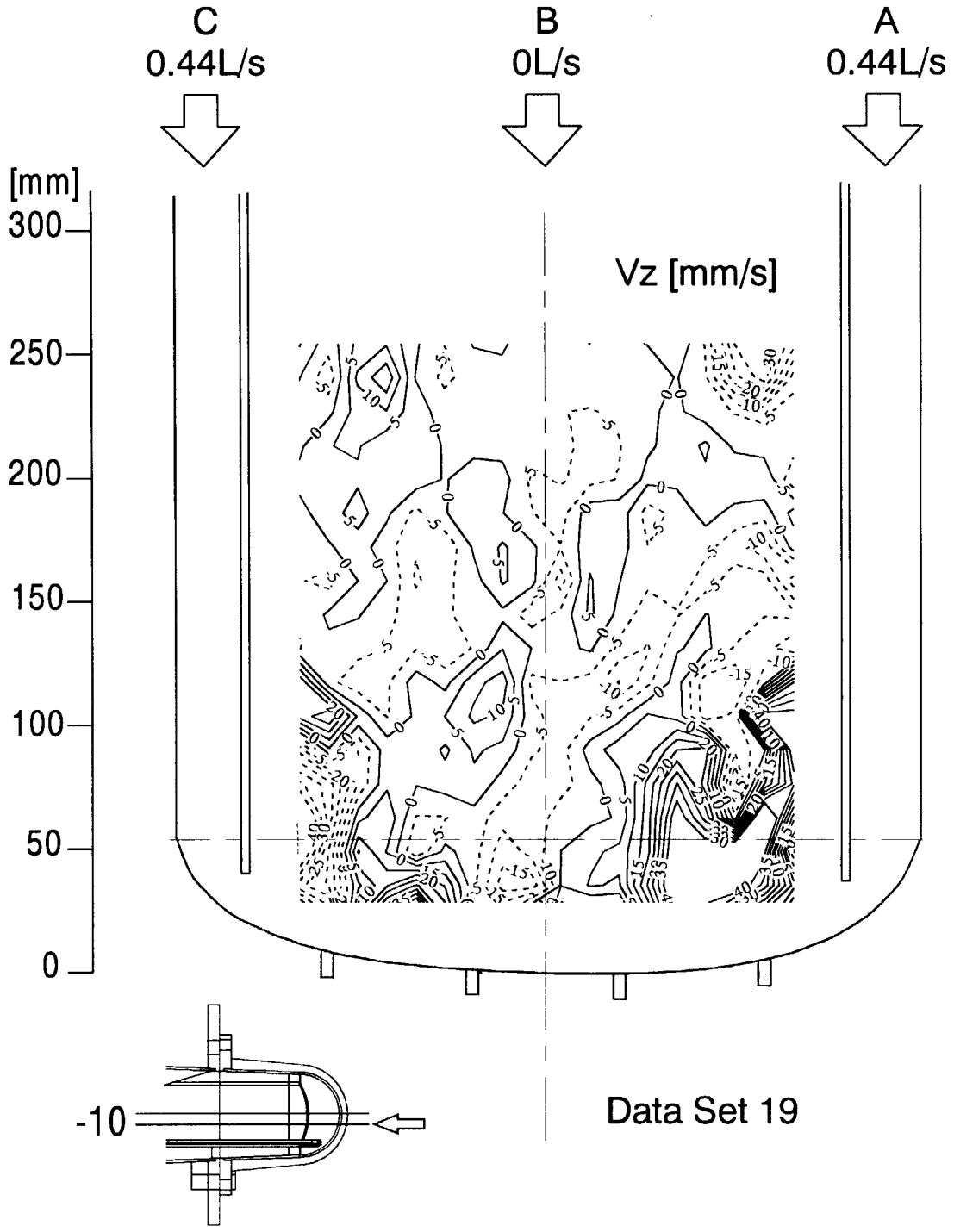

Fig.32 Calculated Vz Contour Map (1 : 0 : 1)

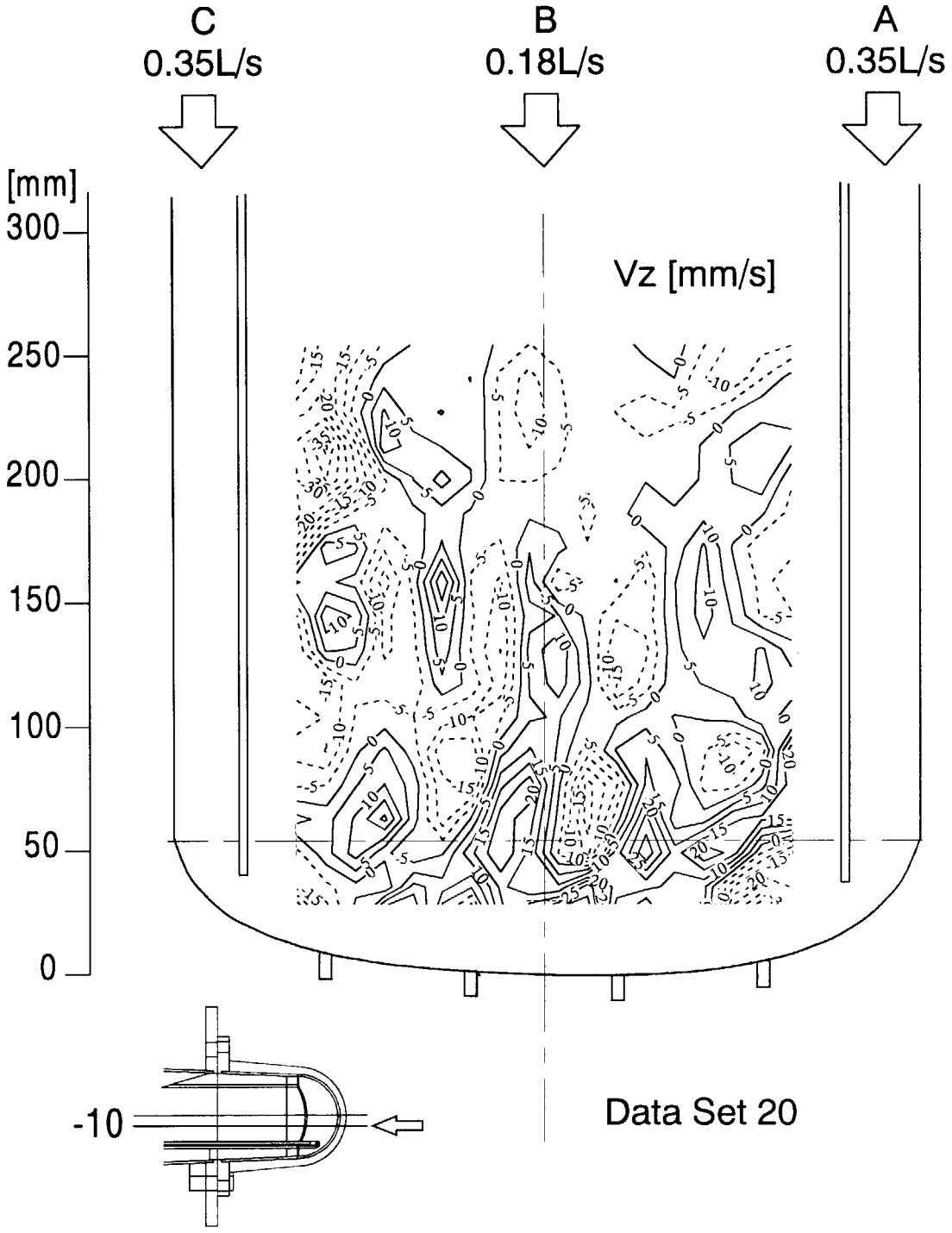

Fig.33 Calculated Vz Contour Map (2 : 1 : 2)

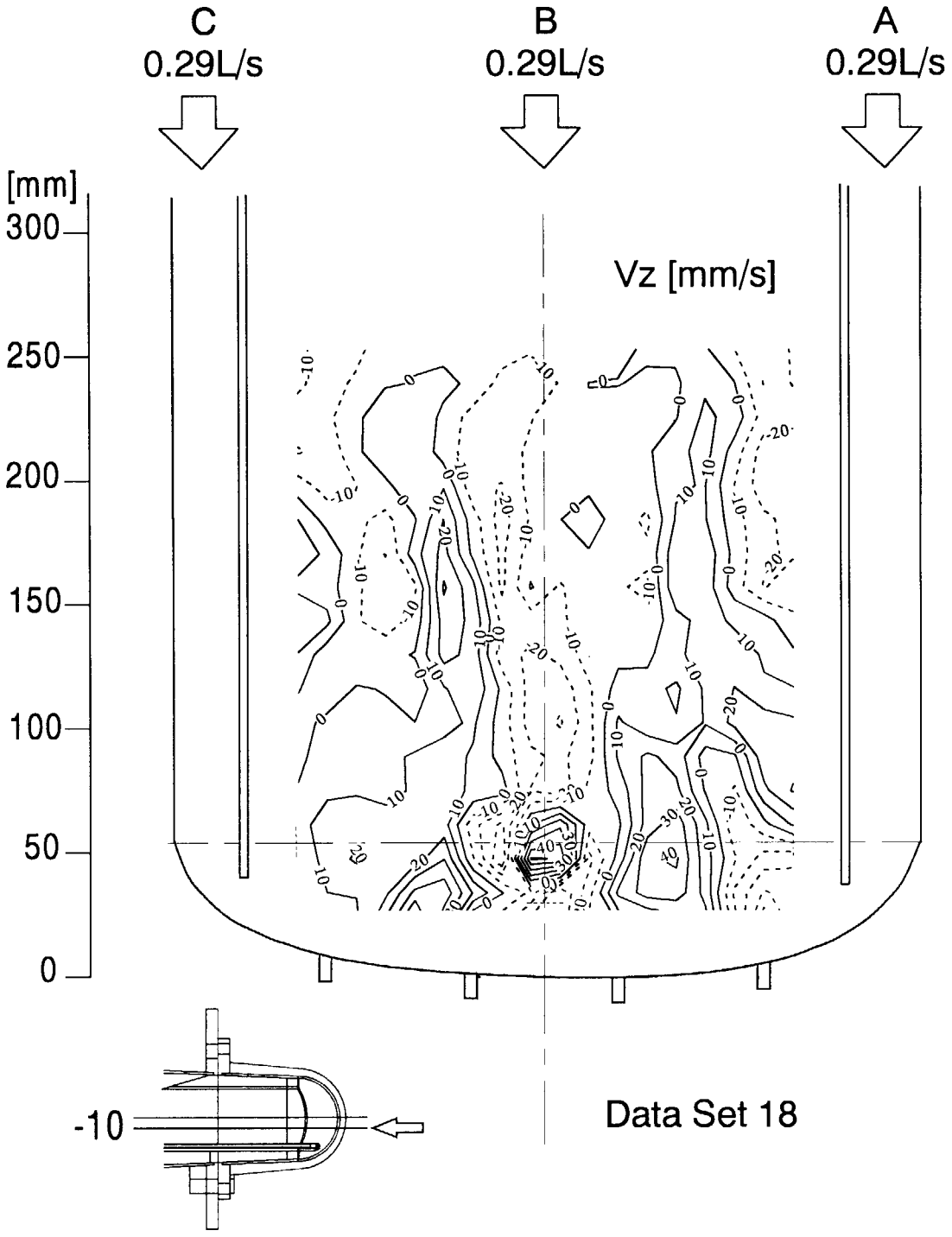

Fig.34 Calculated Vz Contour Map (1 : 1 : 1)

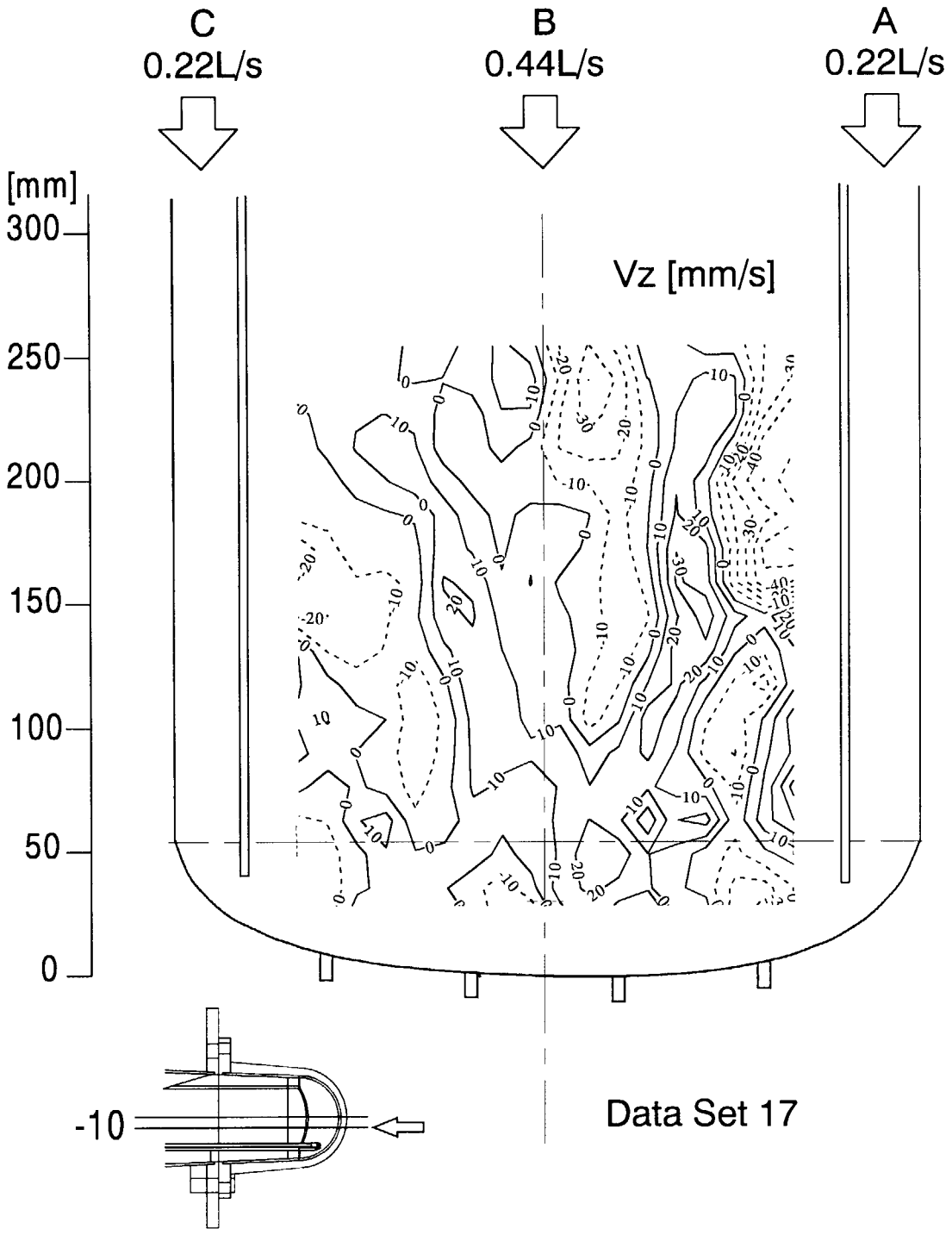

Fig.35 Calculated Vz Contour Map (1 : 2 : 1)

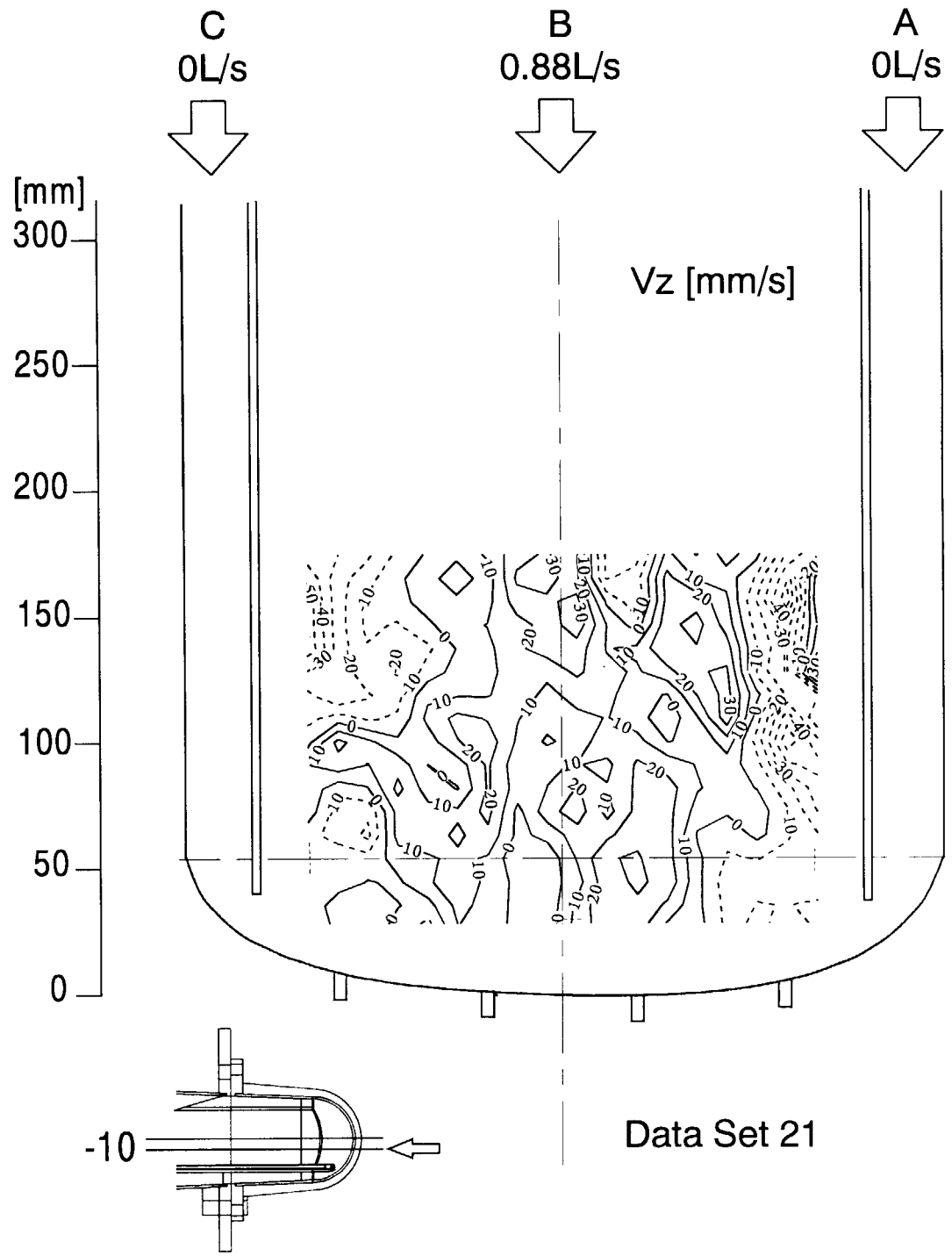

Fig.36 Calculated Vz Contour Map (0 : 1 : 0)

This is a blank page.

国際単位系 (SI) と換算表

表 1　SI基本単位および補助単位

量	名称	記号
長さ	メートル	m
質量	キログラム	kg
時間	秒	s
電流	アンペア	A
熱力学温度	ケルビン	K
物質量	モル	mol
光度	カンデラ	cd
平面角	ラジアン	rad
立体角	ステラジアン	sr

表 2　SIと併用される単位

名称	記号
分，時，日	min，h，d
度，分，秒	°，′，″
リットル	l，L
トン	t
電子ボルト	eV
原子質量単位	u

1 eV = 1.60218 × 10^{-19} J

1 u = 1.66054 × 10^{-27} kg

表 5　SI接頭語

倍数	接頭語	記号
10^{18}	エクサ	E
10^{15}	ペタ	P
10^{12}	テラ	T
10^{9}	ギガ	G
10^{6}	メガ	M
10^{3}	キロ	k
10^{2}	ヘクト	h
10^{1}	デカ	da
10^{-1}	デシ	d
10^{-2}	センチ	c
10^{-3}	ミリ	m
10^{-6}	マイクロ	μ
10^{-9}	ナノ	n
10^{-12}	ピコ	p
10^{-15}	フェムト	f
10^{-18}	アト	a

表 3　固有の名称をもつSI組立単位

量	名称	記号	他のSI単位による表現
周波数	ヘルツ	Hz	s^{-1}
力	ニュートン	N	$m \cdot kg/s^2$
圧力，応力	パスカル	Pa	N/m^2
エネルギー，仕事，熱量	ジュール	J	N·m
工率，放射束	ワット	W	J/s
電気量，電荷	クーロン	C	A·s
電位，電圧，起電力	ボルト	V	W/A
静電容量	ファラド	F	C/V
電気抵抗	オーム	Ω	V/A
コンダクタンス	ジーメンス	S	A/V
磁束	ウェーバ	Wb	V·s
磁束密度	テスラ	T	Wb/m^2
インダクタンス	ヘンリー	H	Wb/A
セルシウス温度	セルシウス度	℃	
光束	ルーメン	lm	cd·sr
照度	ルクス	lx	lm/m^2
放射能	ベクレル	Bq	s^{-1}
吸収線量	グレイ	Gy	J/kg
線量当量	シーベルト	Sv	J/kg

表 4　SIと共に暫定的に維持される単位

名称	記号
オングストローム	Å
バーン	b
バール	bar
ガル	Gal
キュリー	Ci
レントゲン	R
ラド	rad
レム	rem

1 Å = 0.1 nm = 10^{-10} m

1 b = 100 fm^2 = 10^{-28} m^2

1 bar = 0.1 MPa = 10^5 Pa

1 Gal = 1 cm/s^2 = 10^{-2} m/s^2

1 Ci = 3.7 × 10^{10} Bq

1 R = 2.58 × 10^{-4} C/kg

1 rad = 1 cGy = 10^{-2} Gy

1 rem = 1 cSv = 10^{-2} Sv

（注）

1. 表1－5は「国際単位系」第5版，国際度量衡局 1985年刊行による。ただし，1 eVおよび1 uの値はCODATAの1986年推奨値によった。
2. 表4には海里，ノット，アール，ヘクタールも含まれているが日常の単位なのでここでは省略した。
3. barは，JISでは流体の圧力を表わす場合に限り表2のカテゴリーに分類されている。
4. EC閣僚理事会指令ではbar，barnおよび「血圧の単位」mmHgを表2のカテゴリーに入れている。

換算表

力	N(=10^5 dyn)	kgf	lbf
	1	0.101972	0.224809
	9.80665	1	2.20462
	4.44822	0.453592	1

粘度　1 Pa·s(N·s/m^2) = 10 P(ポアズ)(g/(cm·s))

動粘度　1 m^2/s = 10^4 St(ストークス)(cm^2/s)

圧力	MPa(=10 bar)	kgf/cm^2	atm	mmHg(Torr)	lbf/in^2(psi)
	1	10.1972	9.86923	7.50062 × 10^3	145.038
	0.0980665	1	0.967841	735.559	14.2233
	0.101325	1.03323	1	760	14.6959
	1.33322 × 10^{-4}	1.35951 × 10^{-3}	1.31579 × 10^{-3}	1	1.93368 × 10^{-2}
	6.89476 × 10^{-3}	7.03070 × 10^{-2}	6.80460 × 10^{-2}	51.7149	1

エネルギー・仕事・熱量	J(=10^7 erg)	kgf·m	kW·h	cal(計量法)	Btu	ft·lbf	eV
	1	0.101972	2.77778 × 10^{-7}	0.238889	9.47813 × 10^{-4}	0.737562	6.24150 × 10^{18}
	9.80665	1	2.72407 × 10^{-6}	2.34270	9.29487 × 10^{-3}	7.23301	6.12082 × 10^{19}
	3.6 × 10^6	3.67098 × 10^5	1	8.59999 × 10^5	3412.13	2.65522 × 10^6	2.24694 × 10^{25}
	4.18605	0.426858	1.16279 × 10^{-6}	1	3.96759 × 10^{-3}	3.08747	2.61272 × 10^{19}
	1055.06	107.586	2.93072 × 10^{-4}	252.042	1	778.172	6.58515 × 10^{21}
	1.35582	0.138255	3.76616 × 10^{-7}	0.323890	1.28506 × 10^{-3}	1	8.46233 × 10^{18}
	1.60218 × 10^{-19}	1.63377 × 10^{-20}	4.45050 × 10^{-26}	3.82743 × 10^{-20}	1.51857 × 10^{-22}	1.18171 × 10^{-19}	1

1 cal = 4.18605 J (計量法)

= 4.184 J (熱化学)

= 4.1855 J (15 °C)

= 4.1868 J (国際蒸気表)

仕事率　1 PS (仏馬力)

= 75 kgf·m/s

= 735.499 W

放射能	Bq	Ci
	1	2.70270 × 10^{-11}
	3.7 × 10^{10}	1

吸収線量	Gy	rad
	1	100
	0.01	1

照射線量	C/kg	R
	1	3876
	2.58 × 10^{-4}	1

線量当量	Sv	rem
	1	100
	0.01	1

（86年12月26日現在）

FLOW STUDY ON THE ESS TARGET WATER MODEL USING THE UVP METHOD